ELECTRONIC PROPERTIES OF CORRELATED IMPURITIES IN TWO DIMENSIONAL MATERIALS

A Thesis Submitted to
the Graduate School of
İzmir Institute of Technology
in Partial Fulfillment of the Requirements for the Degree of

MASTER OF SCIENCE

in Physics

by
Volkan DOLU

October 2023

İZMİR

We approve the thesis of **Volkan DOLU**

Examining Committee Members:

Assoc. Prof. Dr. Özgür ÇAKIR
Department of Physics, İzmir Institute of Technology

Prof. Dr. Alev Devrim GÜÇLÜ
Department of Physics, İzmir Institute of Technology

Assoc. Prof. Dr. Ümit AKINCI
Department of Physics, Dokuz Eylül University

20 / 10 / 2023

Assoc. Prof. Dr. Özgür ÇAKIR
Supervisor, Department of Physics,
İzmir Institute of Technology

Prof. Dr. Lütfi ÖZYÜZER
Head of the Department of
Physics

Prof. Dr. Mehtap EANES
Dean of the Graduate School

ACKNOWLEDGMENTS

I would like to extend my sincere thanks to Özgür Çakır for his invaluable patience and support.

I also had great pleasure of working with Harun Gökalp.

ABSTRACT

ELECTRONIC PROPERTIES OF CORRELATED IMPURITIES IN TWO DIMENSIONAL MATERIALS

This Master's thesis investigates the effects of single and dual impurity potentials on the electronic properties of both pristine and gapped graphene, being examples of two-dimensional materials. The behavior of 2D materials at the atomic levels, particularly graphene, has been of interest due to their particular electronic properties, such as high electron mobility at certain conditions. The presence of impurities may significantly influence these properties, providing a modifiable platform for rearranging electronic characteristics for diverse applications.

Our research focuses on how the impurity states that emerge, especially around energies at low DOS, affect the electronic structure and the interaction between the impurities. We study these effects in the presence of both single and dual impurity potentials of varied strength using computational models based on tight-binding approach. We begin by looking at how the single impurity potentials affect the electronic properties of pristine graphene and gapped graphene. We analyze the change in DOS and energy of the system, along with the identification of the impurity states, utilizing participation ratio for localization. Then, we extend our study to dual impurity potentials and their impacts to provide a knowledge of multi-impurity scenarios. We explore the interaction of the impurities mediated by the Fermi sea. In particular, we studied the hybridization of impurity states and corresponding impurity energies. Next, we determine the force arising between impurities for various Fermi energies, impurity-impurity distances and impurity potential strengths for graphene and gapped graphene.

ÖZET

İKİ BOYUTLU MALZEMELERDE İLİŞKİLİ SAFSIZLIKLARIN ELEKTRONİK ÖZELLİKLERİ

Bu yüksek lisans tezi, tek ve ikili safsızlık potansiyellerinin, iki boyutlu malzeme örneği olan grafen ve bant aralıklı grafenin elektronik özellikleri üzerindeki etkilerini araştırmaktadır. İki boyutlu malzemelerin, özellikle de grafenin atom seviyesindeki davranışı, belirli koşullar altında yüksek elektron hareketliliği gibi belirli elektronik özelliklerinden dolayı ilgi çekici olmuştur. Safsızlıkların varlığı bu özellikleri önemli ölçüde etkileyebilir ve çeşitli uygulamalar için elektronik özelliklerin yeniden düzenlenmesi için değiştirilebilir bir platform sağlayabilir. Araştırmamız, özellikle düşük durum yoğunluğundaki enerjiler etrafında ortaya çıkan safsızlık durumlarının elektronik yapıyı ve safsızlıklar arasındaki etkileşimi anlamaya odaklanmaktadır. Bu etkileri, 'tight-binding' yaklaşımına dayalı hesaplama modelleri kullanarak, çeşitli büyüklüklerdeki hem tekli hem de ikili safsızlık potansiyellerinin varlığında inceliyoruz. Tek safsızlık potansiyellerinin grafenin ve bant aralıklı grafenin elektronik özelliklerini nasıl etkilediğine bakarak başlıyoruz. Daha sonra, çoklu safsızlık senaryoları hakkında bilgi sağlamak için çalışmamızı ikili safsızlık potansiyellerini ve bunların etkilerini kapsayacak şekilde genişletiyor ve Fermi denizinin aracılığıyla oluşan safsızlık potansiyellerinin etkileşimlerini araştırıyoruz. Özellikle, safsızlık durumlarının hibridizasyonunu ve bunlara karşılık gelen safsızlık enerjilerini inceledik. Daha sonra, grafen ve bant aralıklı grafen için, safsızlıklar arasında ortaya çıkan kuvveti çeşitli Fermi enerjileri, safsızlıklar arası mesafe ve potansiyel güçlerine göre belirleyerek analiz ediyoruz.

TABLE OF CONTENTS

LIST OF FIGURES

LIST OF TABLES

Table **Page**

CHAPTER 1

Introduction

2D materials, sometimes referred to as single layer materials, are crystalline materials consisting of a single layer of atoms. Graphene, commonly associated with 2D materials, is one of the most studied examples of these materials, while there are many others these days, such as hexagonal boron nitride (h-BN), phosphorene and silicene. Graphene, a two-dimensional hexagonal lattice of carbon atoms, has attracted extensive interest in the field of condensed matter physics due to its special electronic properties. Its unique band structure and transport characteristics have led to various applications, ranging from nanoelectronics to energy storage devices. Understanding the electronic behavior of graphene under different conditions is essential for exploring its potential applications and improving its performance.

The theoretical foundations of graphene can be traced back to 1947, when Wallace demostrated the unusual semi-metallic behavior of this material in his valuable work "The Band Theory of Graphite" (Wallace, 1947). Diamond and graphite were considered to be the only two physical forms of carbon until the mid-1980s (Seekaew et al., 2019). Boehm et al. proposed the name "graphene" in 1986 by combining the words graphite with the suffix "en" (Boehm et al., 1994). A historic moment in graphene research occurred in 2004, when Novoselov et al. synthesized graphene using the micromechanical cleavage technique (Novoselov et al., 2004). Given the significance of this achievement for physics and materials research, Novoselov and Geim were awarded the Nobel Prize in Physics in 2010. Graphene has great potential for both scientific and technological applications due to its unique electronic properties, such as high electron mobility and thermal conductivity. This potential spans a spectrum of applications, from ultra-high frequency transistors and gas sensors to transparent flexible electrode materials (Wehling et al., 2009).

In recent years, the investigation of the electronic properties of graphene has extended beyond pristine systems to include the effects of impurities and defects. Impurity potentials, resulting from adsorbed atoms or vacancies in the lattice, can significantly modify the electronic structure and transport properties of graphene(Wehling et al., 2009). Therefore, understanding the impact of these impurities on graphene's electronic behavior is of great importance. Furthermore, the physics of graphine exhibits interesting phe-

nomena such that its low energy excitations are massless, Chiral, and Dirac fermions (Castro Neto et al., 2009). The interaction between impurities in graphene can be described as a fermionic version of the Casimir interaction, with massless fermions acting as photons. Depending on whether the impurities are on the same sublattice or on different sublattices, the interaction will be either attractive or a repulsive (Shytov et al., 2009). This gives the possibility of adjusting the sign of the impurity interaction through Fermi energy modifications (Lebohec et al., 2014). In the presence of impurities and defects in a electronically conducting medium induces perturbations due to the scattering of its electrons. These variations in electronic scattering emerge as spatial oscillations known as Friedel oscillations (Lawlor et al., 2013). The introduction of magnetic impurities in graphene has created an exciting field for researchers. These impurities can induce local magnetic moments, leading to potential applications in spintronics (Uchoa and Castro Neto, 2007). Furthermore, the interaction between these magnetic moments and graphene's π electrons can lead to various many-body effects, including potential magnetic ordering or the emergence of the Kondo effect (Wehling et al., 2008).

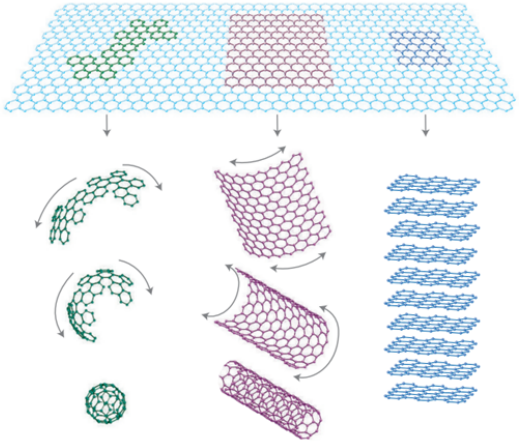

Figure 1.1: Construction of materials from Graphene for different dimensions. (Geim and Novoselov, 2007).

In this Master's thesis, we focus on studying the electronic effects of impurity potentials on a sample graphene bulk. The toroidal geometry is chosen to simulate the behavior of graphene samples by imposing periodic boundary conditions. The system consists of a torus-shaped graphene sheet, which can be represented as a periodic array of unit cells as a finite-sized system. In order to better understand the electronic properties of a 2D material like graphene, two impurities have been studied as a further step along with a single impurity.

To investigate the electronic properties of this system, we employ a tight-binding model, which accurately captures the quantum mechanical behavior of electrons in graphene. The tight-binding Hamiltonian provides a computationally efficient framework for simulating the electronic structure and transport properties of graphene-based systems. We utilize Matlab, a powerful numerical computing environment, to construct and solve the tight-binding Hamiltonian for the graphene sheet.

The primary objectives of this thesis are as follows:

* Constructing the tight-binding Hamiltonian for the torus-shaped graphene bulk as a finite-sized system.

* Introducing a single impurity potential within the lattice and studying its electronic effects on the graphene system.

* Analyzing the modification of the electronic band structure and density of states due to the impurity potential along with the total energy change of the system by adjusting fermi level.

* Investigating the total energy changes in the system consists of two impurities by determining the localized states for various impurity potentials.

* Determining the attractive and repulsive interactions between impurity states for different potential strengths and adjusted fermi levels that emerge from the existence of two impurity potentials.

By achieving these objectives, we aim to provide insights into the electronic behavior of graphene in the presence of impurities, contributing to the fundamental understanding of graphene physics and its potential applications

In the subsequent chapters, we will present the theoretical background of graphene, the tight-binding model, and the methodology used to construct the tight-binding Hamiltonian for the torus-shaped graphene bulk. We will then discuss the results obtained from our simulations and provide a comprehensive analysis of the effects on electronic properties induced by the impurity potentials. Finally, we will draw conclusions based on our findings and propose future directions for further investigation.

Overall, this Master's thesis aims to contribute to the growing body of knowledge on the electronic behavior of graphene, specifically focusing on the impact of impurity potentials in a finite-sized graphene sheet obeying boundary conditions.

1.1 Graphene

Graphene is a two-dimensional crystal with a periodic arrangement of atoms extending along both the x and y axes in the plane. The honeycomb lattice of graphene consists of two carbon atoms per unit cell, labelled A and B as scetched in Fig.1.2. The graphene unit cell is thus described as a two-atom basis with hexagonal lattice symmetry. Three valance electrons of carbon,- out of four, make sp^2(sigma bonds) bonding with their nearest neighbors. Remaining unpaired one electron in p_z orbital feels weak periodic potential and moves almost freely in graphene.

To begin with, we define the lattice vectors, or primitive vectors, of the graphene unit cell. These vectors, denoted as $\boldsymbol{a_1}$ and $\boldsymbol{a_2}$, point from one lattice point to another. They are typically chosen to form the edges of the unit cell, with each vector spanning from one carbon atom to another. The primitive vectors can be written as:

$$\boldsymbol{a_1} = a\left(\frac{\sqrt{3}}{2}, \frac{3}{2}\right) \qquad \boldsymbol{a_2} = a\left(-\frac{\sqrt{3}}{2}, \frac{3}{2}\right) \tag{1.1}$$

where a is the lattice constant which is approximately 1.42 A^0 which is the distance between two adjacent carbon atoms in graphene.

The reciprocal lattice is a lattice in reciprocal space, i.e., in momentum space; which is very important for understanding several phenomena in the context of solid-state physics. The corresponding reciprocal lattice vectors, denoted $\boldsymbol{b_1}$ and $\boldsymbol{b_2}$, are given by:

$$\boldsymbol{b_1} = \frac{2\pi}{3a}\left(\sqrt{3}, 1\right) \qquad \boldsymbol{b_2} = \frac{2\pi}{3a}\left(-\sqrt{3}, 1\right) \tag{1.2}$$

As shown in Fig.1.3 there are three $\boldsymbol{K}$ and $\boldsymbol{K'}$ points at the corners of graphene Brillouin zone (BZ). These crucial points are also named Dirac points. They are as follows:

$$\boldsymbol{K} = \frac{2\pi}{3a}\left(\frac{\sqrt{3}}{3}, 1\right) \qquad \boldsymbol{K'} = \frac{2\pi}{3a}\left(-\frac{\sqrt{3}}{3}, 1\right) \tag{1.3}$$

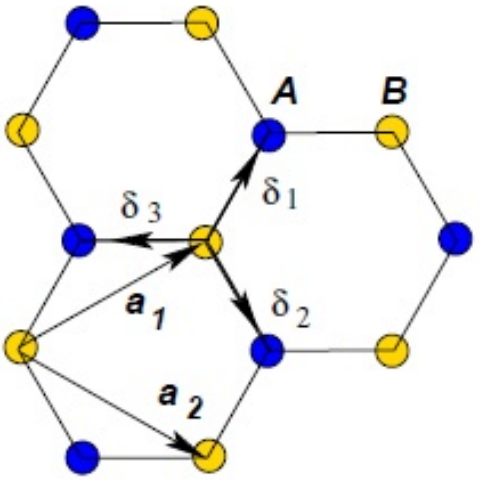

Figure 1.2: Lattice structure of graphene with A and B sites labeled. δ_1, δ_2 and δ_3 are nearest neighbor vectors (Castro Neto et al., 2009).

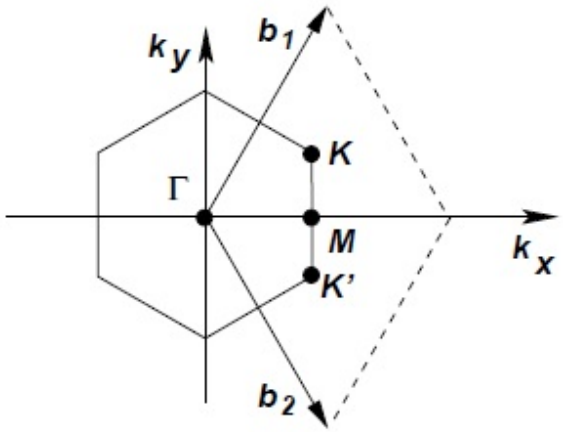

Figure 1.3: Burillioun zone of graphene with Dirac poins K, K' and zone center Γ point (Castro Neto et al., 2009).

1.2 Tight-binding Hamiltonian

The tight-binding model is a mathematical framework used to describe the electronic structure of a solid. Considering nearest neighbor hopping (NN) t_1 and next-nearest neighbor hopping (NNN) t_2, the tight-binding Hamiltonian for graphene is

$$\hat{H} = \sum_i \varepsilon_o \left(\hat{a}_i^\dagger \hat{a}_i + \hat{b}_i^\dagger \hat{b}_i\right) - t_1 \sum_{\langle i,j\rangle} \left(\hat{a}_i^\dagger \hat{b}_j + \hat{b}_j^\dagger \hat{a}_i\right)) - t_2 \sum_{\langle\langle i,j\rangle\rangle} \left(\hat{a}_i^\dagger \hat{a}_j + \hat{b}_i^\dagger \hat{b}_j + h.c.\right), \quad (1.4)$$

where $i(j)$ labels sites in sublattice $A(B)$, the fermionic operator $\hat{a}_i^\dagger$ ($\hat{a}_i$) creates (annihilates) an electron at the A site whose position is $\mathbf{r}_i$, and $\hat{b}_j^\dagger \left(\hat{b}_j\right)$ acts similarly for B sublattice, ε_o (set to 0 for simplicity) is the on-site energy. Additionally, "h.c." stands for "Hermitian conjugate." which is $\hat{a}_j^\dagger \hat{a}_i + \hat{b}_j^\dagger \hat{b}_i$ in (1.4). We can rewrite the sum over nearest neighbors as

$$\sum_{\langle i,j\rangle} \left(\hat{a}_i^\dagger \hat{b}_j + \hat{b}_j^\dagger \hat{a}_i\right) = \sum_{i\in A} \sum_\delta \left(\hat{a}_i^\dagger \hat{b}_{i+\delta} + \hat{b}_{i+\delta}^\dagger \hat{\delta}_i\right) \quad (1.5)$$

where the sum over δ is carried out over the nearest-neighbor vectors δ_1, δ_2, and $\boldsymbol{\delta}_3$, and the operator $\hat{b}_{i+\delta}$ annihilates a fermion at the B site whose position is $\mathbf{r}_i + \boldsymbol{\delta}$. Using

$$\hat{a}_i^\dagger = \frac{1}{\sqrt{N/2}} \sum_{\mathbf{k}} e^{i\mathbf{k}\cdot\mathbf{r}} \hat{a}_{\mathbf{k}}^\dagger, \quad (1.6)$$

where $N/2$ is the number of A sites, and similarly for $\hat{b}_{i+\delta}^\dagger$, we can write the tight-binding Hamiltonian for graphene (1.4) including only NN interactions by taking $t_2 = 0$ as

$$\begin{aligned}\hat{H} &= -\frac{t_1}{N/2}\sum_{i\in A}\sum_{\delta,\mathbf{k}\mathbf{k}'}\left[e^{i(\mathbf{k}-\mathbf{k}')\cdot\mathbf{r}_i}e^{-i\mathbf{k}'\cdot\delta}\hat{a}^\dagger_{\mathbf{k}}\hat{b}_{\mathbf{k}'} + \text{ h.c. }\right] \\ &= -t_1\sum_{\delta,\mathbf{k}}\left(e^{-i\mathbf{k}\cdot\delta}\hat{a}^\dagger_{\mathbf{k}}\hat{b}_{\mathbf{k}} + \text{ h.c. }\right) \\ &= -t_1\sum_{\delta,\mathbf{k}}\left(e^{-i\mathbf{k}\cdot\delta}\hat{a}^\dagger_{\mathbf{k}}\hat{b}_{\mathbf{k}} + e^{i\mathbf{k}\cdot\delta}\hat{b}^\dagger_{\mathbf{k}}\hat{a}_{\mathbf{k}}\right),\end{aligned} \tag{1.7}$$

where in the second line we have used

$$\sum_{i\in A} e^{i(\mathbf{k}-\mathbf{k}')-\mathbf{r}_\mathbf{i}} = \frac{N}{2}\delta_{\mathbf{k}\mathbf{k}'}. \tag{1.8}$$

The Hamiltonian can now be represented as

$$\hat{H} = \sum_{\mathbf{k}} \Psi^\dagger \mathbf{h}(\mathbf{k})\Psi \tag{1.9}$$

where

$$\Psi \equiv \begin{pmatrix} \hat{a}_{\mathbf{k}} \\ \hat{b}_{\mathbf{k}} \end{pmatrix}, \quad \Psi^\dagger = \begin{pmatrix} \hat{a}^\dagger_{\mathbf{k}} & \hat{b}^\dagger_{\mathbf{k}} \end{pmatrix} \tag{1.10}$$

The matrix form of the Hamiltonian will be

$$\mathbf{h}(\mathbf{k}) \equiv -t_1\begin{pmatrix} 0 & \Delta_{\mathbf{k}} \\ \Delta^*_{\mathbf{k}} & 0 \end{pmatrix} \tag{1.11}$$

with

$$\Delta_{\mathbf{k}} \equiv \sum_{\delta} e^{i\mathbf{k}\cdot\delta}. \tag{1.12}$$

The eigenvalues of $\mathbf{h}(\mathbf{k})$ are $E_{\pm} = \pm t_1\sqrt{\Delta_{\mathbf{k}}\Delta_{\mathbf{k}}^*}$. We can compute this by writing $\Delta_{\mathbf{k}}$ out more explicitly:

$$\begin{aligned}
\Delta_{\mathbf{k}} &= e^{i\mathbf{k}\cdot\delta_1} + e^{i\mathbf{k}\cdot\delta_2} + e^{i\mathbf{k}\cdot\delta_3} \\
&= e^{i\mathbf{k}\cdot\delta_3}\left[1 + e^{i\mathbf{k}\cdot(\delta_1-\delta_3)} + e^{i\mathbf{k}\cdot(\delta_2-\delta_3)}\right] \\
&= e^{-ik_z a}\left[1 + e^{i3k_x a/2}e^{i\sqrt{3}k_y a/2} + e^{i3k_z a/2}e^{-i\sqrt{3}k_y a/2}\right] \\
&= e^{-ik_z a}\left[1 + e^{i3k_x a/2}\left(e^{i\sqrt{3}k_y a/2} + e^{-i\sqrt{3}k_y a/2}\right)\right] \\
&= e^{-ik_z a}\left[1 + 2e^{i3k_x a/2}\cos\left(\frac{\sqrt{3}}{2}k_y a\right)\right].
\end{aligned} \tag{1.13}$$

Thus, the energy bands are given by

$$E_{\pm}(\mathbf{k}) = \pm t_1\sqrt{1 + 4\cos\left(\frac{3}{2}k_x a\right)\cos\left(\frac{\sqrt{3}}{2}k_y a\right) + 4\cos^2\left(\frac{\sqrt{3}}{2}k_y a\right)}, \tag{1.14}$$

or, as it can be written as well,

$$E_{\pm}(\mathbf{k}) = \pm t_1\sqrt{3 + f(\mathbf{k})} \tag{1.15}$$

where

$$f(\mathbf{k}) = 2\cos\left(\sqrt{3}k_y a\right) + 4\cos\left(\frac{3}{2}k_x a\right)\cos\left(\frac{\sqrt{3}}{2}k_y a\right). \tag{1.16}$$

These are two gapless bands that touch at the Dirac points **K** and **K′**. In other words, the Dirac points are the points in **k**-space for which $E_{\pm}(\mathbf{k}) = 0$. The resulting dispersion relation as a graph can be seen in Fig.1.4

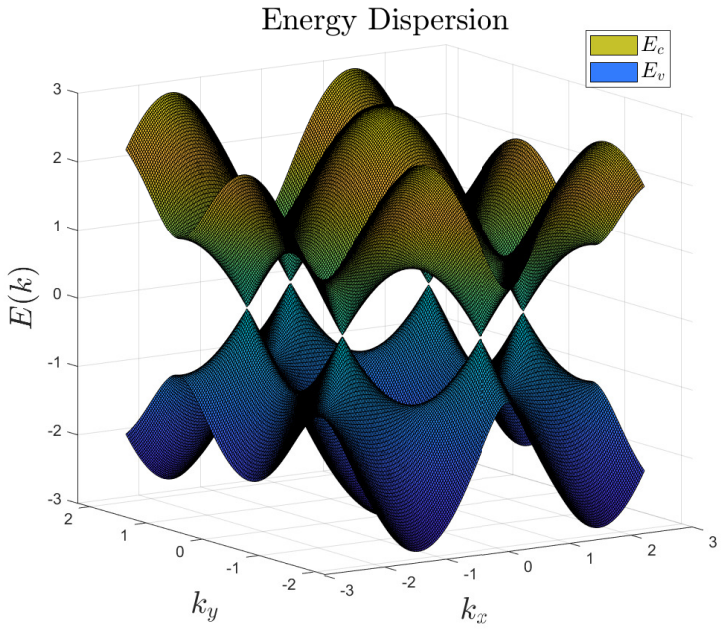

Figure 1.4: Energy bands for graphene from nearest-neighbor interactions. The bands meet at the Dirac points, at which the energy is zero.

CHAPTER 2

Impurities on 2D Material

The electronic properties of graphene are unique due to its special crystal structure, and can be modeled using the tight-binding model. The model offers the ability to numerically build even straightforward models in order to analyze the impact of impurities on graphene. In addition to being of theoretical importance, understanding how impurities affect graphene is crucial for applications that can benefit from its special characteristics. Graphene and gapped graphene have been represented using this method to give a basis for understanding 2D materials. Table 2.1 can be used to have quick snapshot about the covered areas to be analyzed .

Table 2.1: The map of the covered areas for numerical analysis.

	Pure Graphene	Gapped Graphene
Single Impurity	- DOS - Energy by Index - Energy and PR by Strength	- DOS - Energy by Index - Energy and PR by Strength
Two Impurities	DOS - Energy by Index - Energy and PR by Strength - Total Energy - Force between imp. states	DOS - Energy by Index - Energy and PR by Strength - Total Energy - Force between imp. states

2.1 Pristine Graphene

2.1.1 Single Impurity

In this section, the effects of a single impurity on a sample graphene sheet have been studied. Firstly, tight-binding Hamiltonian for the sample has been constructed as a matrix for the numerical analysis. The constructed tight-binding Hamiltonian, H with an impurity has been diagonalized to analyze the effects of impurity on the electronic properties of graphene; such as localized eigenstates, density of states(DOS) and energy changes in the system. In this study the sample is composed of 10000 (100x100) unit cells containing 20000 atoms and the impurity was assumed to be located on $\boldsymbol{A}$ site of the unit cell designated as the sample sheet's initial unit cell. Three input parameters are used to construct H :

- N, the number of atoms in each direction;
- t_1, the hopping parameter (due to NN overlapping);
- V_{imp}, the impurity potential.

Imposing periodic boundary conditions ensures that the electronic states are properly described for a periodic system. Then the hopping matrix construction continued by iterating over all pairs of atoms and setting the off-diagonal elements to $-t_1$ if the distance between the atoms is less than a certain threshold which is the nearest neighbor atoms in this case. Finally, the impurity potential has been added to the diagonal element of H. On-site energies are assumed to be 0 for the simplicity since all atoms are identical in the system. Each lattice site corresponds to an atomic orbital resulting the hamiltonian matrix of size (NxN). Lastly the value of t_1 is set to 1, to allow for easy comparison of the numbers in the study.

Fig. 2.1 aims to help visualize a basic small sample of a lattice structure consisting of 7x7 unit cells in real space coordinates. Fig. 2.2 shows the reciprocal lattice in reciprocal space, which corresponds to the 90° rotated shape of the lattice in real space.

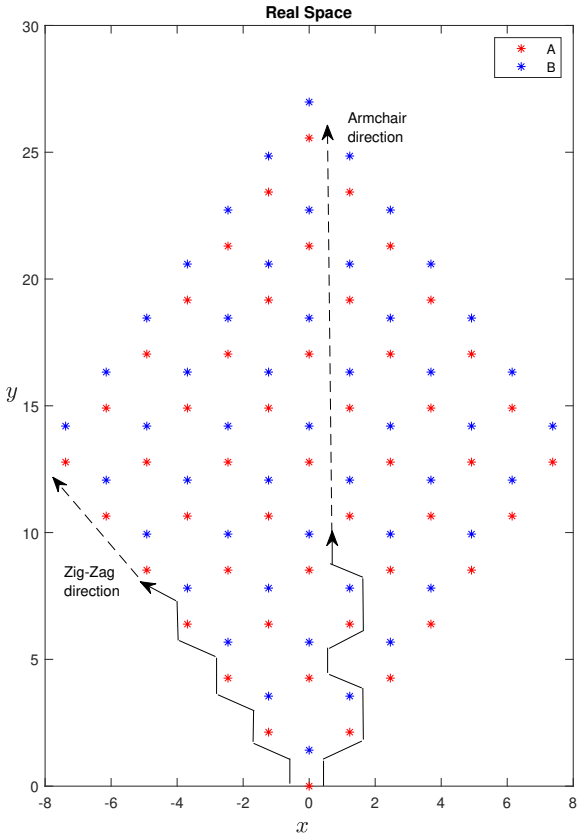

Figure 2.1: Representation of graphene lattice in real space.

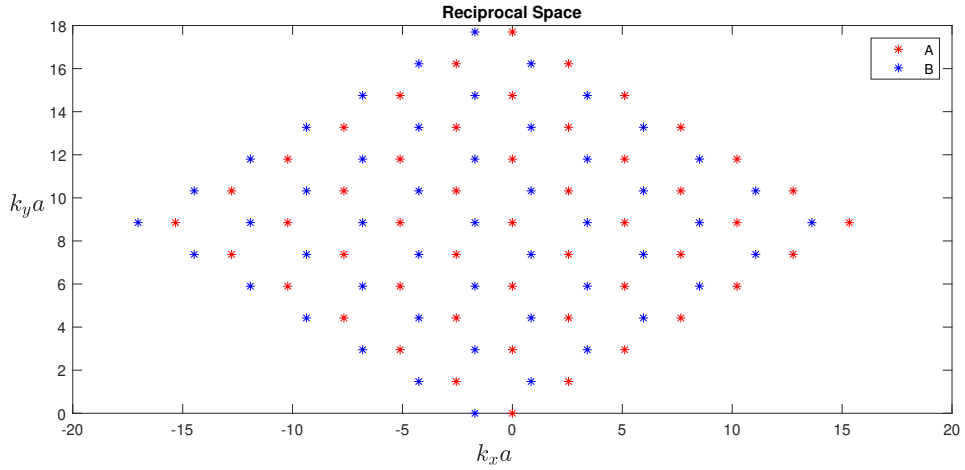

Figure 2.2: Representation of graphene lattice in reciprocal space.

Once having the Hamiltonian matrix ready, now it can be diagonalized to obtain the eigenvalues and eigenvectors. The eigenvalues represent the allowed energy levels, while the corresponding eigenvectors provide information about the electronic wavefunctions and their spatial distribution.

DOS is defined as

$$D(E) = \sum_i \delta(E_i - E) \tag{2.1}$$

by using lorentzian function for a smooth plot

$$L(E) = \frac{1}{\pi} \cdot \frac{\delta}{(E - E_i)^2 + \delta^2} \tag{2.2}$$

we can get the DOS shown in Fig. 2.3a and 2.3b for pure graphene and for graphene with single impurity accordingly.

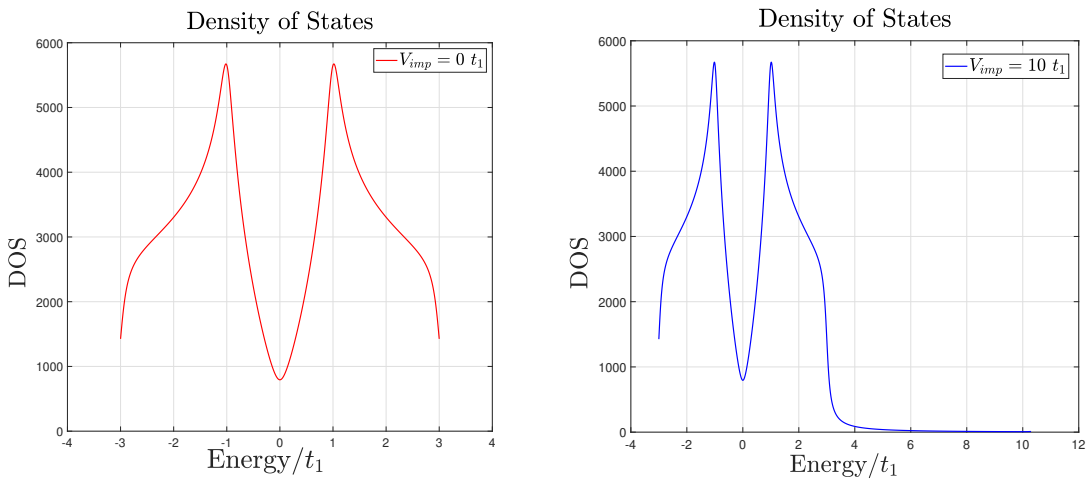

(a) With no impurity (b) With a single impurity; $V_{imp} = 10t_1$

Figure 2.3: DOS using lorentzian with $\delta = 0.1$

In order to visualize the change in DOS around the Fermi energy level δ is set to 0.001 and the plots have been combined with a zoom in part around $E = 0$ in Fig. 2.4 In our numer-

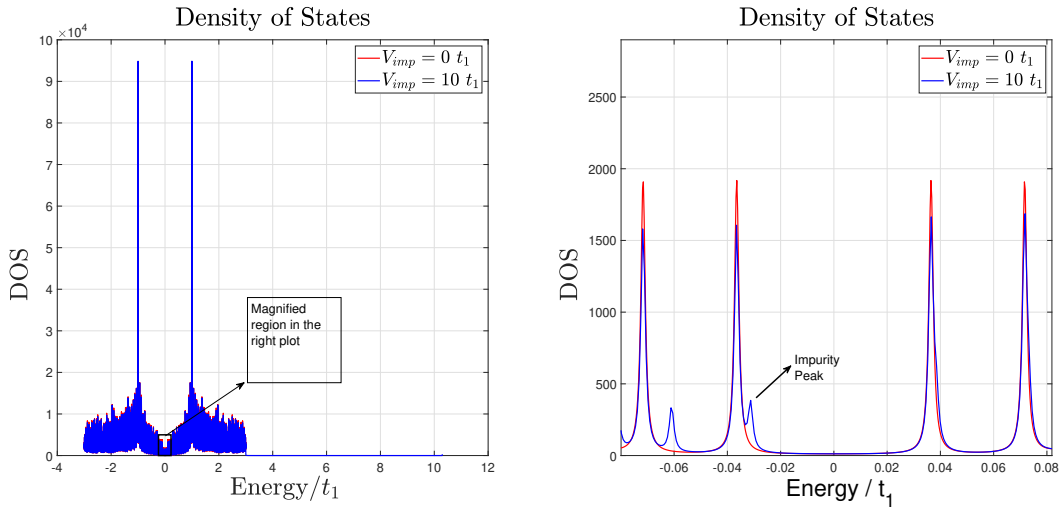

(a) combined form of Fig.2.3a and 2.3b.

(b) Zoomed in region of the plot 2.4a

Figure 2.4: Paired and zoomed region of the Fig.2.3 with $\delta = 0.001$

ical analysis of a single impurity potential on the sample, we observed notable changes in the density of states (DOS) and energy distribution. From the DOS graph, we saw a distinct peak around the Fermi energy level, indicative of the influence of the impurity. We identify this peak as impurity state. In contrast, the pristine graphene exhibited a zero DOS at the Fermi level, characteristic of its semi-metallic behavior. The energy distribution by index plot further provided insights into the scattering effects caused by the impurity (Fig.2.5). A shift in energy levels was seen, supporting the disruption in the electronic structure of graphene. These findings, as visually represented in the provided plots, reinforce the substantial impact of a single impurity on the electronic properties of graphene.

To gain a better understanding of the impact of impurity potential strength on the impurity state that emerges near the Fermi level, energy by strength and participation ratio by strength relationships have been investigated. The participation ratio (PR) is often used as a measure of the localization of a quantum state. It is defined as the the sum of the squares of the probabilities of the state in a given basis. In other words, if a normalized quantum state $|\Psi\rangle$ can be expressed as a linear combination of N basis states $|n\rangle$ with

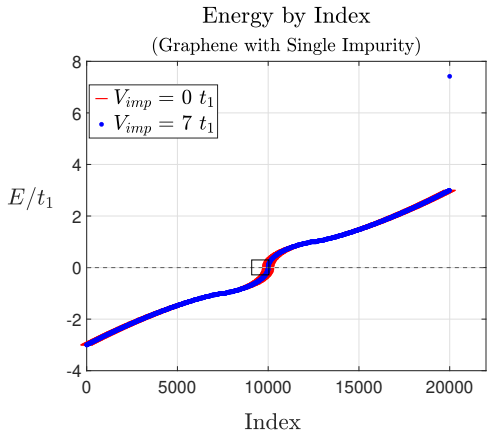

(a) Paired graph of Energy by Index.

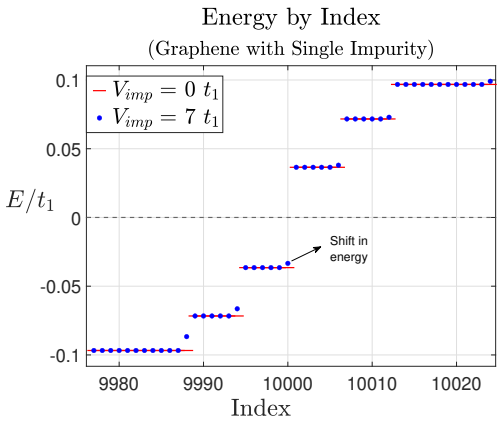

(b) Zoomed in region of the plot 2.5a

Figure 2.5: Paired and zoomed region of Energy by Index graphs

coefficients c_n, then the participation ratio is given by:

$$PR = \sum_n |c_n|^4 \tag{2.3}$$

where $|c_n|^2$ is the probability to find the state in the n^{th} state. A high participation ratio indicates that the state is highly localized in the chosen basis, while a low participation ratio indicates that the state is more delocalized.

To find the localized impurity states, the first five states with the greatest PR were evaluated. The PRs for a few states, despite being higher than the mean PR of all states, cannot be distinguished in the region of V_{imp} between 0 and $10t_1$ in Fig.2.6. However, a state differs from others when the impurity state with highest PR is excluded and focused on the rest four states as shown in Fig.2.7

Once the impurity state has been detected the Fig.2.6 is refined to clearly show the impurity state in Fig.2.8

A graph of the states in real space configuration is plotted to visualize the picture of localizations in Fig. 2.9.

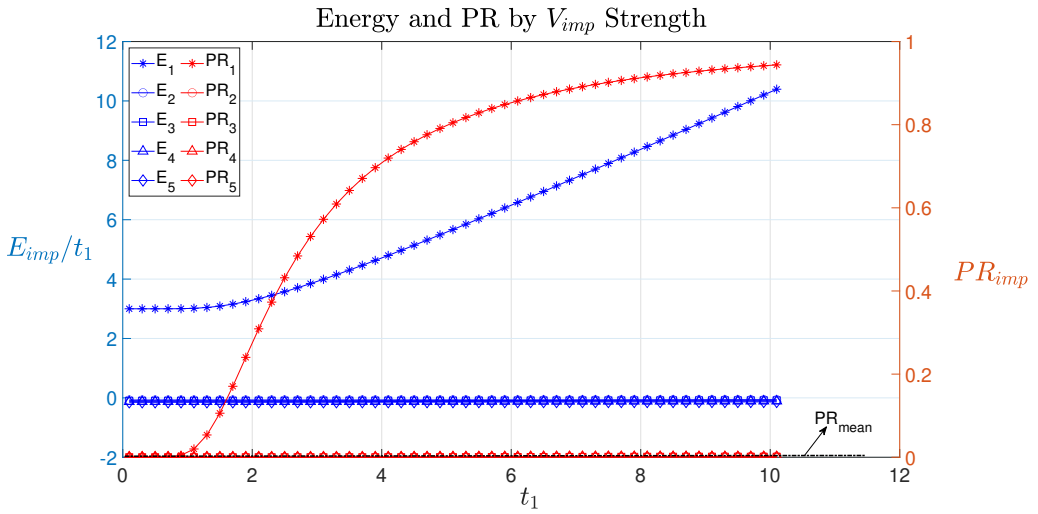

Figure 2.6: Energy and PR by V_{imp} strength between $0 - 10t_1$ for states with the highest five PRs

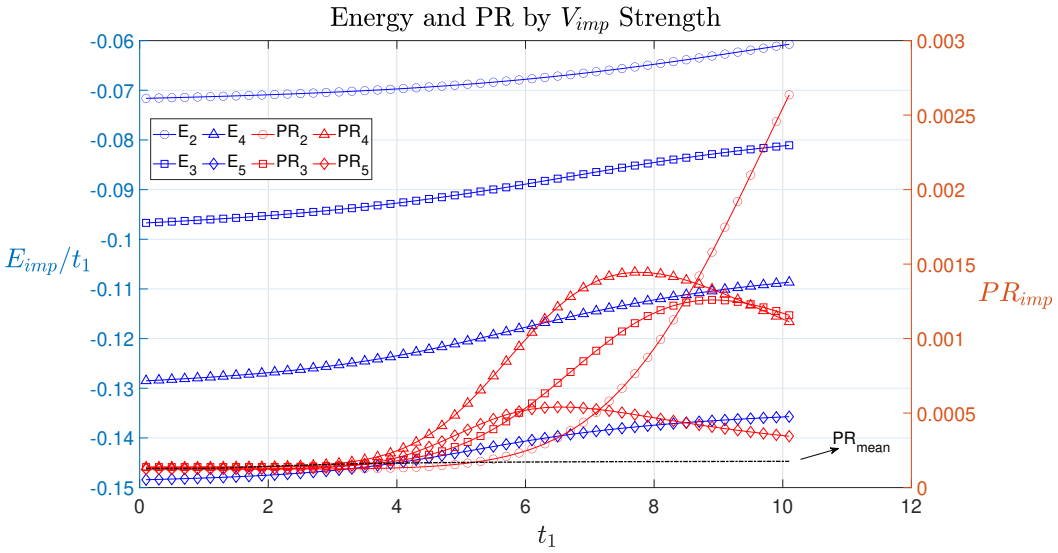

Figure 2.7: Energy and PR by V_{imp} strength between $0 - 10t_1$

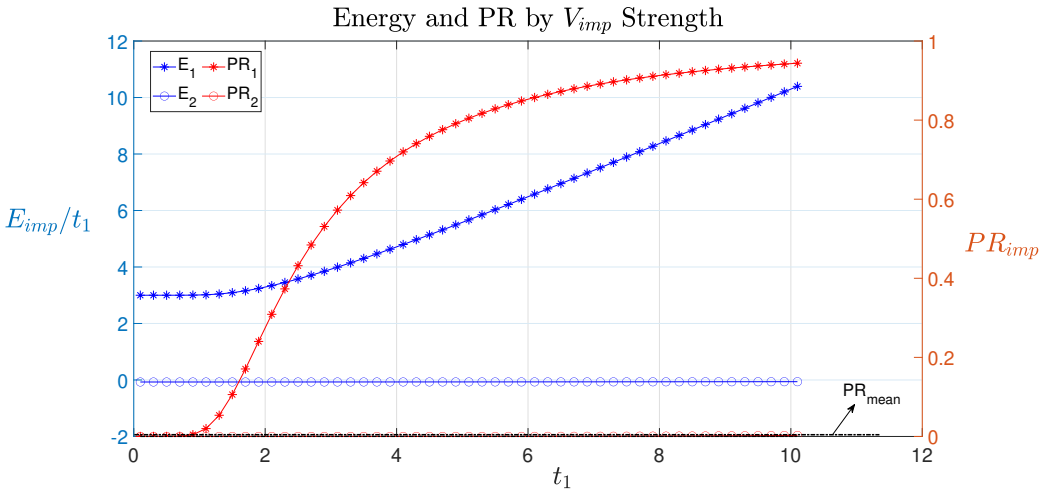

Figure 2.8: Energy and PR by V_{imp} strength between $0 - 10t_1$

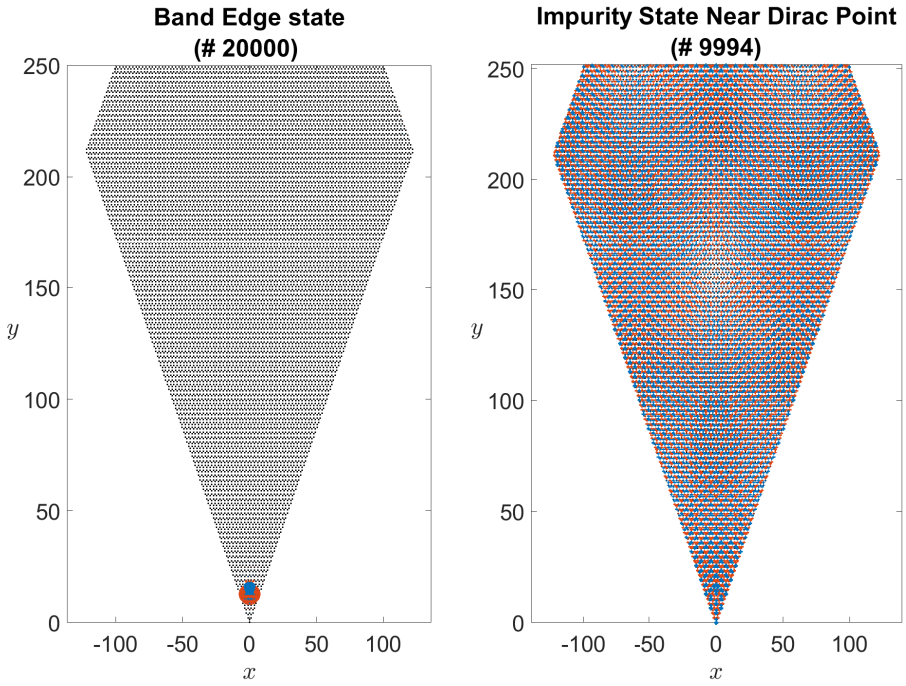

Figure 2.9: The States: 20000 and 9994 in real space lattice for the single impurity potential $V_{imp} = 7t_1$. The circle sizes proportional to the + (blue) and - (red) values.

2.1.2 Two Impurities

A basic model of two impurities has been constructed and examined in order to understand the impact of two impurities on graphene's electronic structure and on each other. To begin, H has been updated to include the second impurity in addition to the first, which is again located at the A site of the initial cell. Both impurity strengths have been set to the same value $V_{imp1} = V_{imp2} = 7t_1$, with all other parameters staying identical from the single impurity example. The addition of a second impurity increases the degree of freedom for the case under examination, which is the position of the second impurity V_{imp2} in relation to V_{imp1}.

In the case of two impurities, DOS and energy by index graphs were created after diagonalizing H to examine the impact of two impurities on the sample. We observed some changes in DOS, especially around $E = 0$, for different impurity potential strengths, as can be seen in the enlarged part of the region in Fig. 2.10. The DOS just below E = 0 increased with increasing potential strengths in accordance with the shifts in the high DOS zones, where the energy is farther from 0. The results, as graphically displayed in the plots, confirm the influence of two impurities on the electronic properties of graphene.

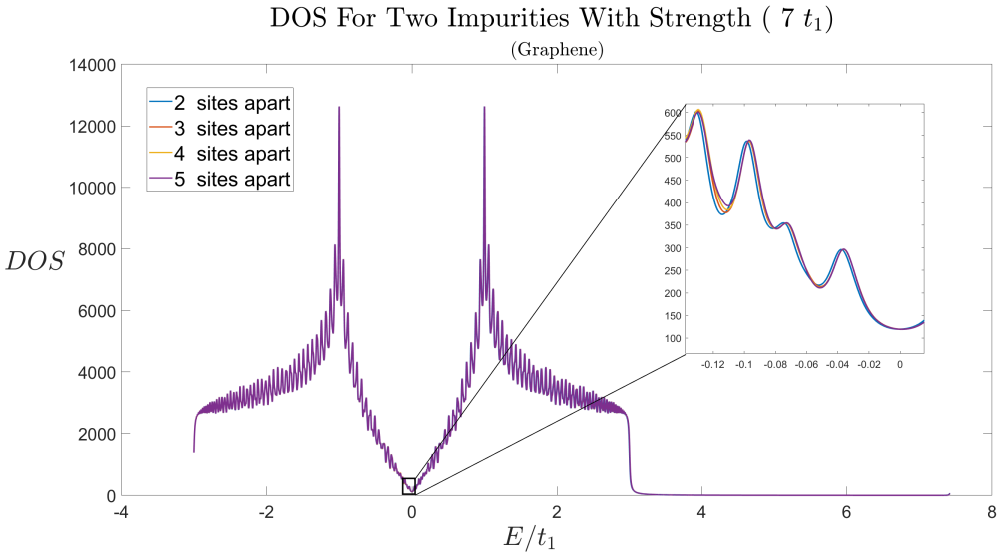

Figure 2.10: Spectrum of DOS of graphene for 4 different distances between $V_{imp1} = 7t_1$ and $V_{imp2} = 7t_1$.

As shown in Fig. 2.11, We observed variations in energy distribution once more while keeping a constant distance between two impurities. To make a better comparison between the effects of single and two impurities on energy levels around $E = 0$, they are plotted on the same graph in Fig.2.12. It can be observed that the single impurity state splits into a pair of impurity states due to the presence of the second impurity. We have identified the pair of impurity states, a doublet, one being the bonding type(E^-) and the other one being the anti-bonding type(E^+).

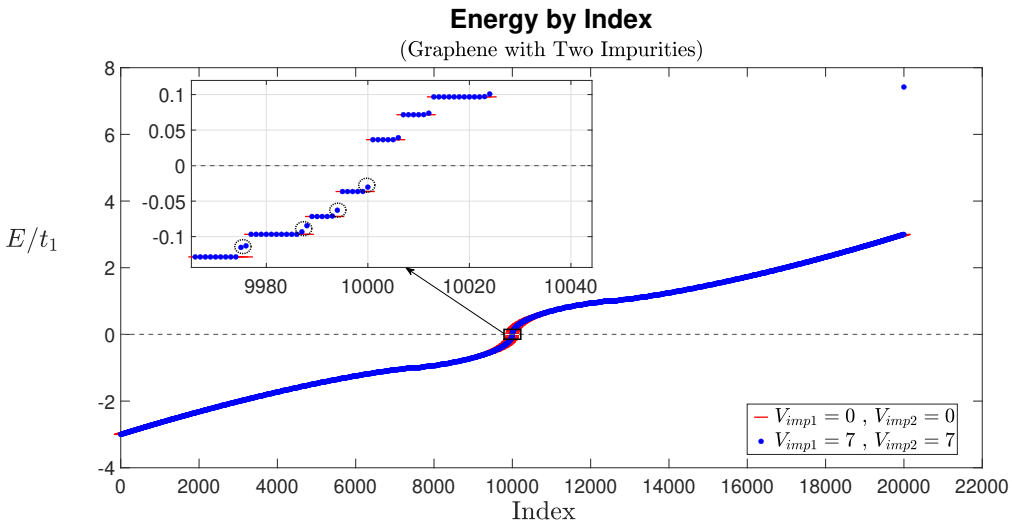

Figure 2.11: Paired and zoomed region of Energy by Index graph.

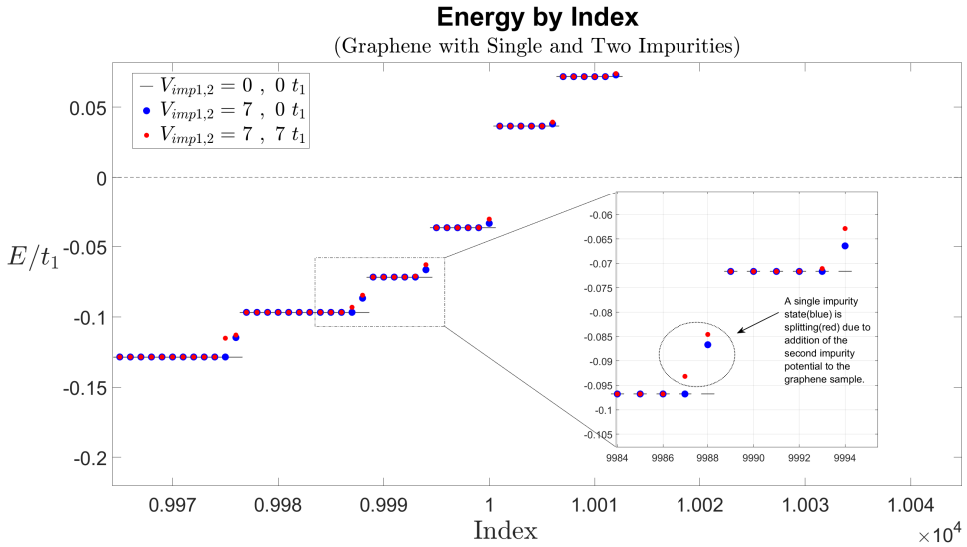

Figure 2.12: Energy by Index for single and two impurities on graphene.

For two impurities, Fig. 2.13 shows the localized impurity states (No: 9994 and 9993) as well as the states (Nos: 20000 and 19999) resulting from the addition of impurities ($V_{imp} = 7t_1$) to the two random A-sites of the sheet.

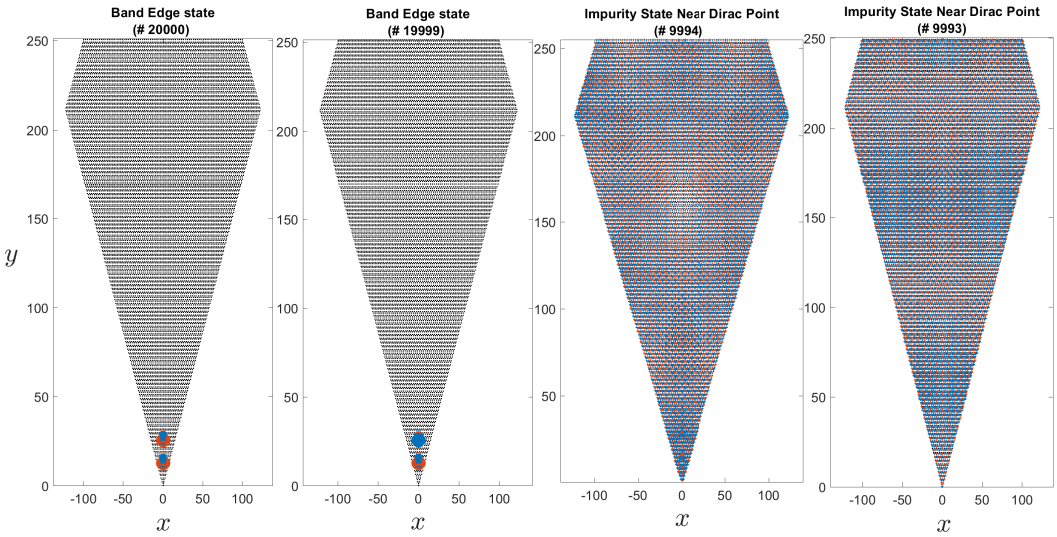

Figure 2.13: Representations in the real space lattice with state no. 20000, 19999, 9994, and 9993 for strength $V_{imp} = 7t_1$. The + (blue) and - (red) values are reflected as the circle sizes.

The energy and PR of a doublet is shown in Fig. 2.14 for the potential strengths from $1t_1$ to $10t_1$ and for the distances between the added impurities, starting from the closest position to the furthest in the armchair direction movement. These 3-D graphs can be used to analyze how energy and PR are in relation to changing strength and distance; two different angles are presented for better examination. Higher energy values and separation can be seen for increasing strength.

In order to have a deeper understanding of the implications of presence of two impurities, energies of doublets have been analysed in a plot along with the total energies determined by E_F set to $E_F < E^-$ for changing distance and for $V_{imp1,2} = 7t_1$. In Fig.2.15, four different doublets around the Dirac point have been combined to see the effects of increasing distance between the impurities. They are labeled Doublet-1, Doublet-2, Doublet-3, and Doublet-4 based on their proximity to the Dirac point. The average energies of the doublets have also been added to the graph to have the insight of splitting the single impurity states after adding the second impurity to the sample graphene sheet.

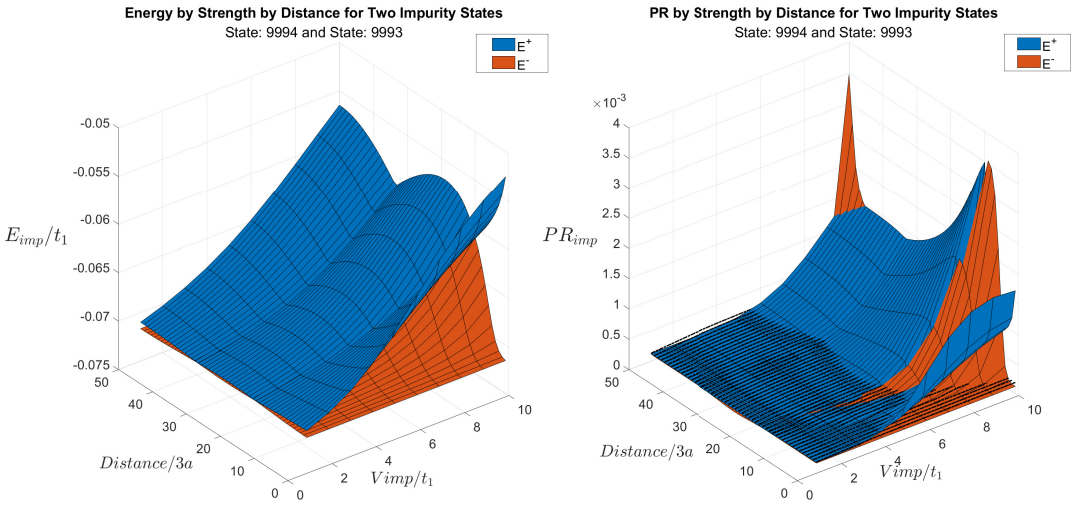

(a) Viewing Angle-1

(b) Viewing Angle-2

Figure 2.14: Impurity State Energy and PR by impurity potential strengths between $0-10t_1$ and by distance between V_{imp1} and V_{imp2} for two viewing angles.

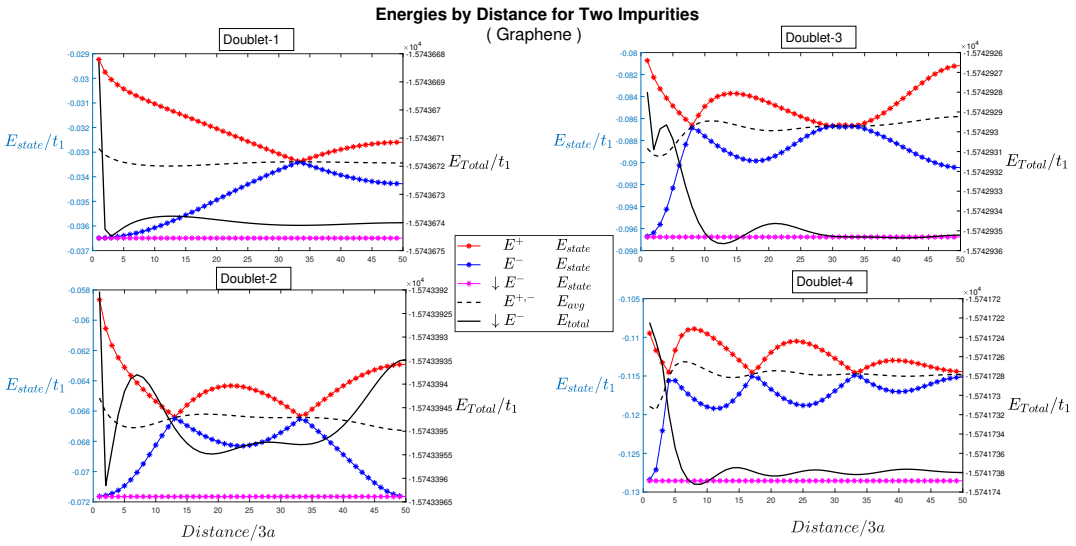

Figure 2.15: Energy by distance for four doublets around Dirac point.

For the impurity states emerged around the Dirac point, the total energy is calculated for three different Fermi levels(E_F) at which the states are filled up with electrons. Fermi levels are arranged according to the energies of the doublet -(just below E^-, between E^- and E^+ and just above E^+). In Fig.2.16, total energy by distance for two doublets which are within the vicinity of the Dirac point can be examined.

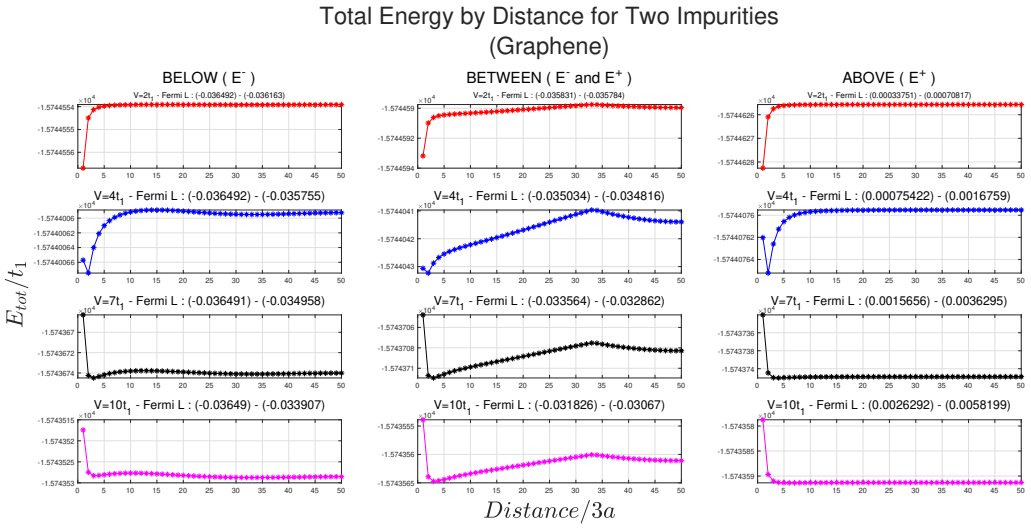

(a) Total Energy in the vicinity of Dirac point: Doublet-1

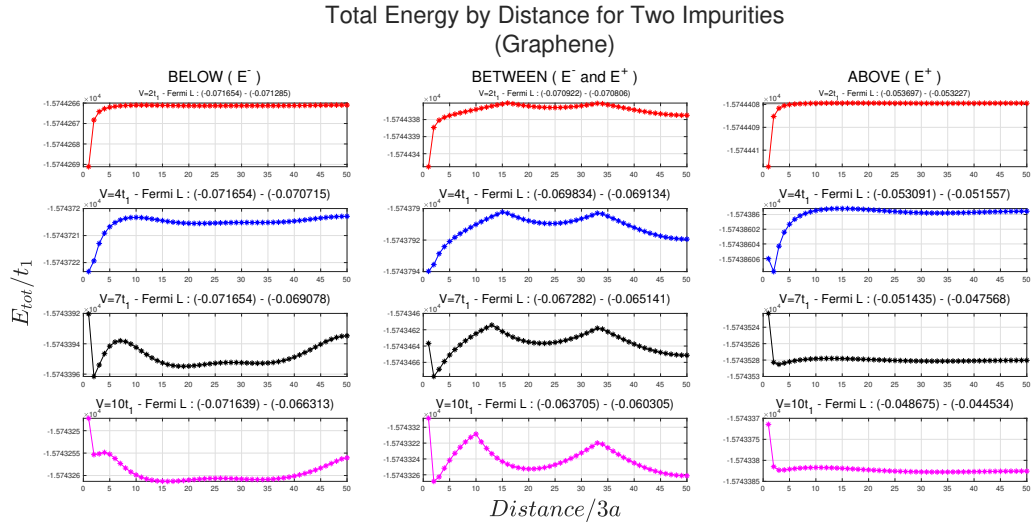

(b) Total Energy in the vicinity of Dirac point: Doublet-2

Figure 2.16: Total energy by distance for several potential strengths where E_F is set in the vicinity of two impurity states.

In the presence of two impurities, the calculated forces for Doublet-1 and Doublet-2, around Dirac point, are plotted in Fig.2.17 where Doublet-2 has the higher PR.

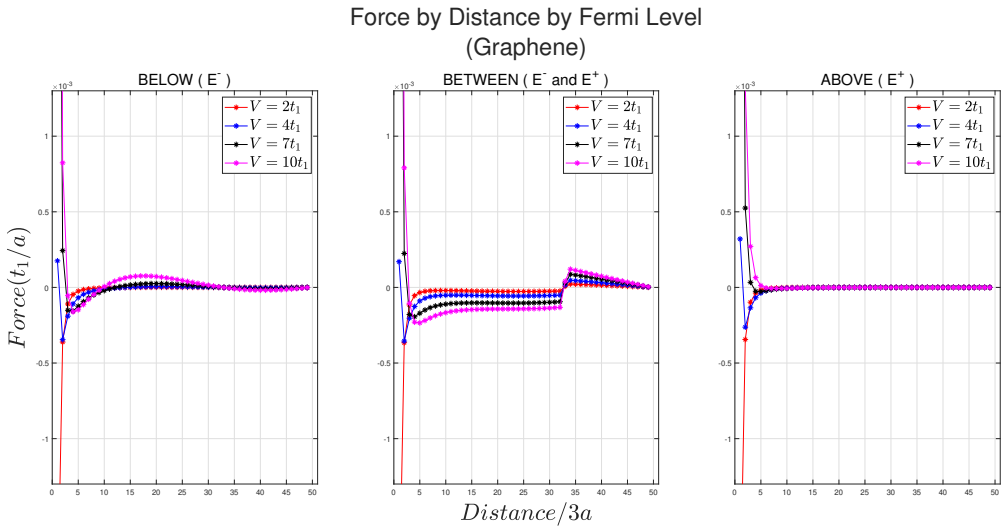

(a) Force by distance: Doublet-1

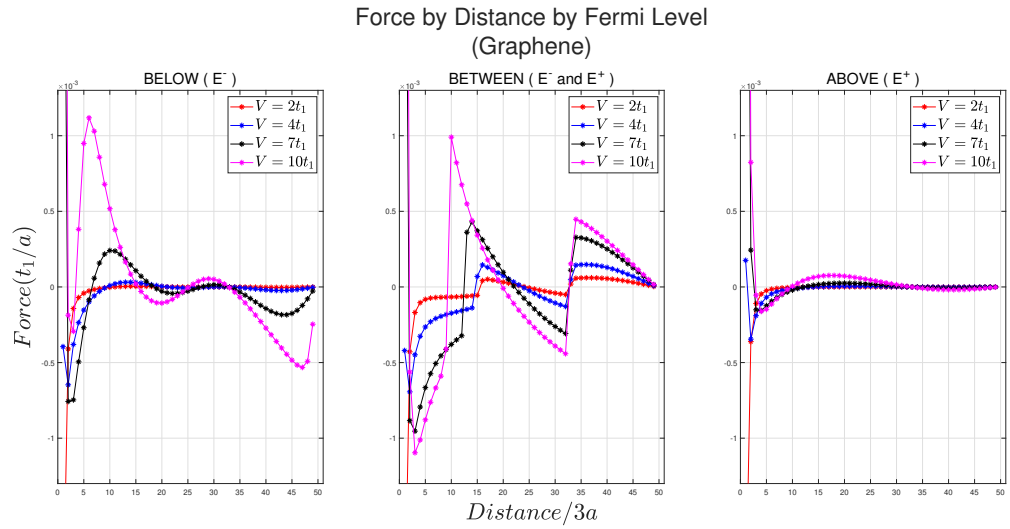

(b) Force by distance: Doublet-2

Figure 2.17: The force between impurities for three different E_F are calculated. In each figure, the impurity strengths, $2t_1$, $4t_1$, $7t_1$, and $10t_1$, are added together for comparison.

The force vanishes at large distances in all cases for Doublet-1. For the situation $E^- < E_F < E^+$, only the bonding orbital is occupied, thus the force is attractive for sufficiently large impurity potentials for Doublet-1. When $E_F < E^-$, which implies that all impurity pairs are occupied, the force is of repulsive character for sufficiently strong impurity potentials. The force strength is rapidly decreasing with increasing distance as

expected in the case of $E_F > E^+$. For Doublet-2 case, Fig. 2.17b, Fermi velocity is non-zero. This leads to Friedel oscillations in total energy and force as well. Note that Friedel oscillations are absent in Fig. 2.17a when Fermi wavevector is zero.

In a similar manner, The forces derived from the total energy for the doublets near Dirac point are represented in Fig.2.18 to display the same information focusing on the impurity strengths enclosing different E_F values. In order to reveal the bonding/anti-bonding character of the two impurity states, Fermi energy is set as $E_F < E^-$, $E^- < E_F < E^+$ and $E_F > E^+$.

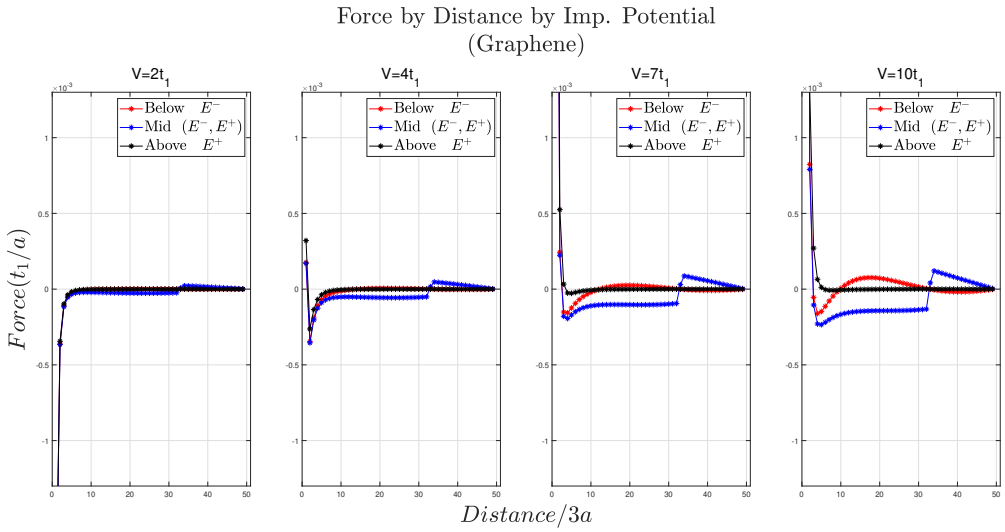

(a) Force by distance: Doublet-1

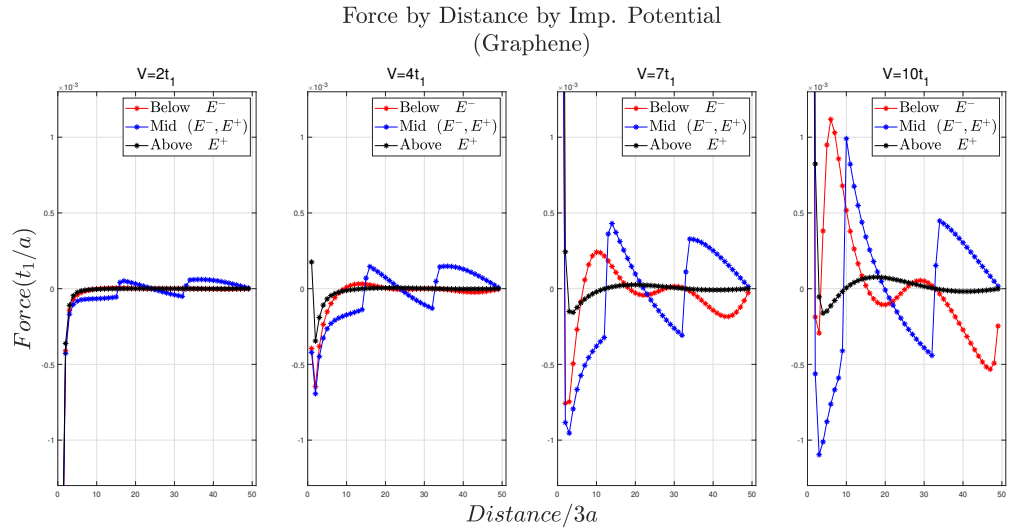

(b) Force by distance: Doublet-2

Figure 2.18: The force between impurity states for four different impurity strengths are calculated. In each figure, Fermi levels; $E_F < E^-$, $E^- < E_F < E^+$ and $E_F > E^+$ are combined in the plot for comparison.

2.2 Gapped Graphene

Although graphene's massless charge carriers make it possible for high electron mobility and other interesting quantum effects, the absence of a natural bandgap limits the material's potential use in a variety of disciplines. Graphene that has been modified to include an energy gap is known as gapped graphene. This can be achieved through applying a perpendicular electric field to bilayer graphene (a structure composed of two layers of graphene), doping it with certain impurities, or mechanically straining the graphene lattice. The creation of a bandgap in graphene opens up a range of potential applications, because it enables the material to have semiconductor-like properties.

By making the appropriate Hamiltonian adjustments, the model created for graphene in section 1 has also been employed in this section of the study for gapped graphene. This was accomplished by updating the diagonal elements of the H matrix with $\pm\Delta\varepsilon/2$, where $\Delta\varepsilon$ is the energy difference between sublattices A and B, used as ε_o for both sites in Eq. 1.4.

Dispersion relation of gapped graphene for $\Delta\varepsilon = 0.25t_1$ can be seen in Fig.2.19

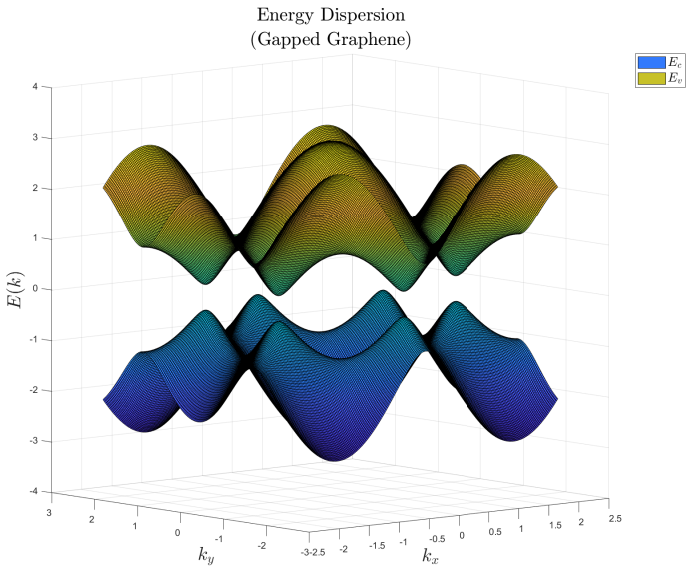

Figure 2.19: Energy bands for graphene with a bandgap formation, as named gapped graphene.

2.2.1 Single Impurity

A single impurity atom can have a significant effect on the electronic properties of gapped graphene, similar to the situation in pure graphene. The specific effect will depend on several factors, including the type of impurity atom, its position in the lattice, and the nature of the gapped graphene, such as on-site energy difference in unit cell.

After diagonalizing H, for $\Delta\varepsilon = 0.25t_1$, DOS and Energy by index were examined. Fig.2.20 shows the change in DOS around $E = 0$.

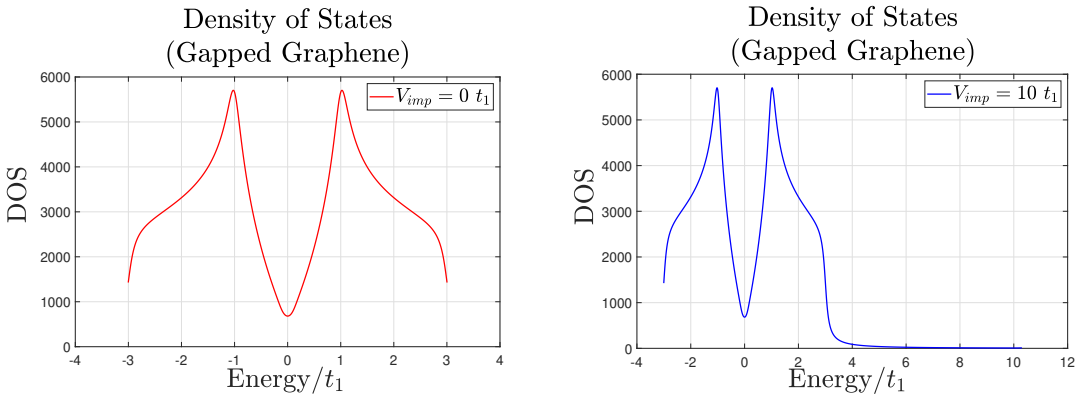

(a) With no impurity

(b) With a single impurity; $V_{imp} = 10t_1$

Figure 2.20: Gapped graphene DOS using lorentzian with $\delta = 0.1$

By looking at the merged graph with $\delta = 0.001$ in lorentzian, the impurity state can be observed in Fig. 2.21. The impurity state appears very close to $E = 0$ within the bandgap due to single impurity potential as shown in Fig. 2.22.

Fig. 2.23 shows how the impurity state set apart from mean Participation Ratio with increasing potential strength. The energy of the state is increasing and approaching to zero by increasing strength as well.

The graph of the states in real space configuration is plotted to get a visualize the picture of localizations in Fig 2.24.

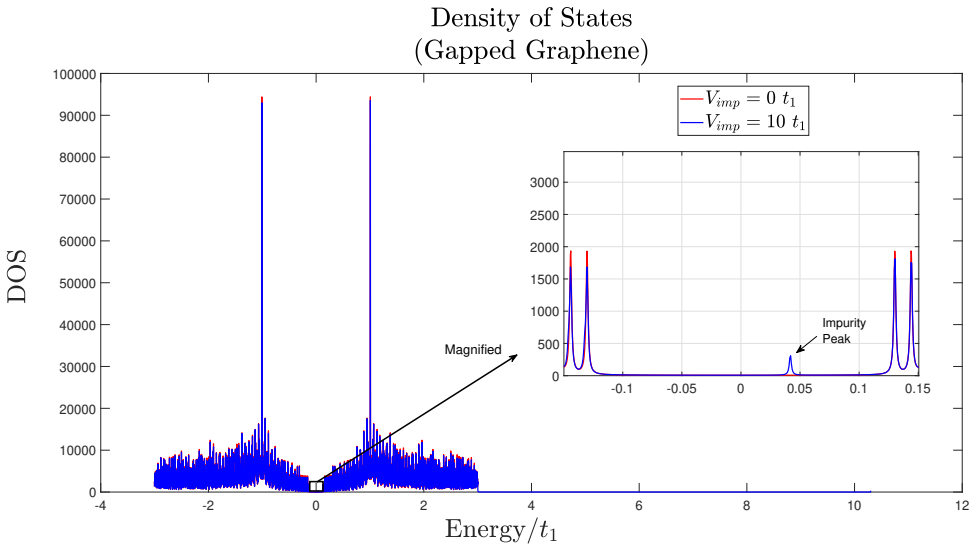

Figure 2.21: Paired and zoomed region with $\delta = 0.001$

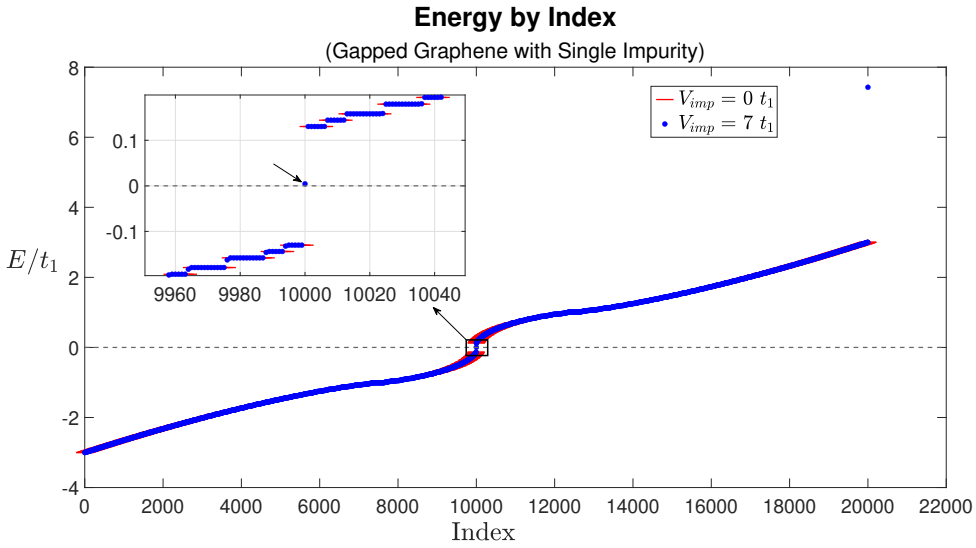

Figure 2.22: Energy by Index graph with enlarged region.

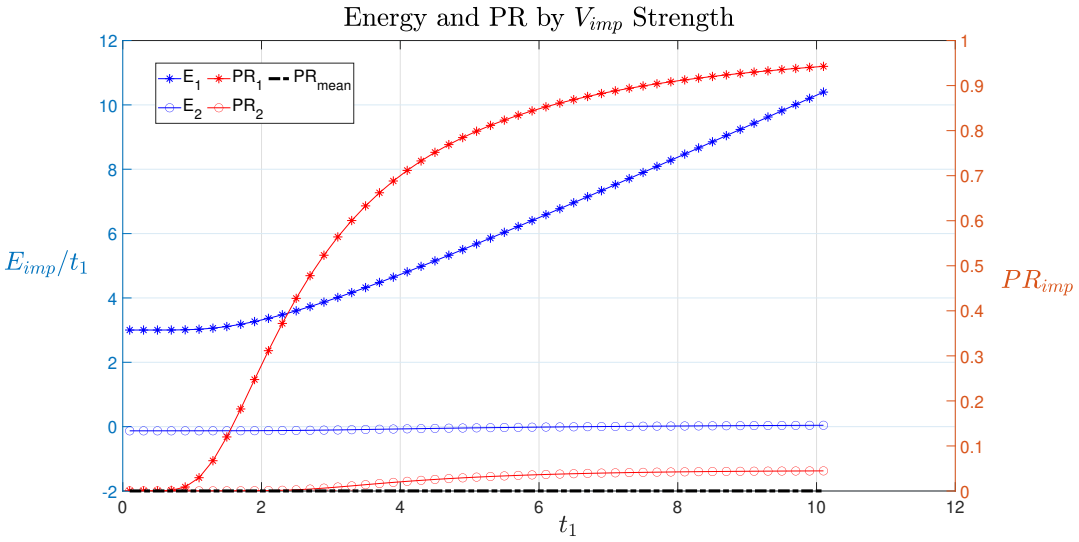

Figure 2.23: Energy and PR by V_{imp} strength between $0 - 10t_1$

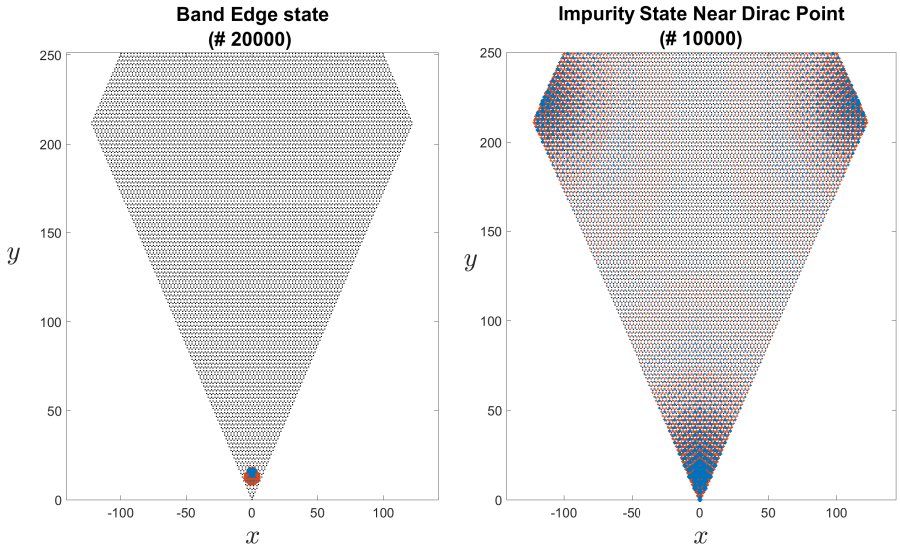

Figure 2.24: The States: 20000 and 10000 in real space lattice for the single impurity potential $V_{imp} = 7t_1$. The circle sizes proportional to the + (blue) and - (red) values.

2.2.2 Two Impurities

Similar to the single impurity case, two impurities can introduce localized states into the graphene lattice. The impurities may interact with each other, depending on the strength and relative position between the them. This interaction can make changes on the electronic properties of the system, including its band structure and electrical conductivity. Additionally, each impurity can also act as a scattering center, potentially leading to further changes in the transport properties of the graphene. Depending on the type and position of the impurities, their effects on the bandgap of gapped graphene could either combine or compete with each other. This could potentially lead to a more significant modulation of the bandgap.

Energy of the gapped graphene system has been examined to identify the energy levels of impurity states emerged. Two states emerged at very close range to $E = 0$ as shown in Energy by index for gapped graphene plot in Fig.2.25.

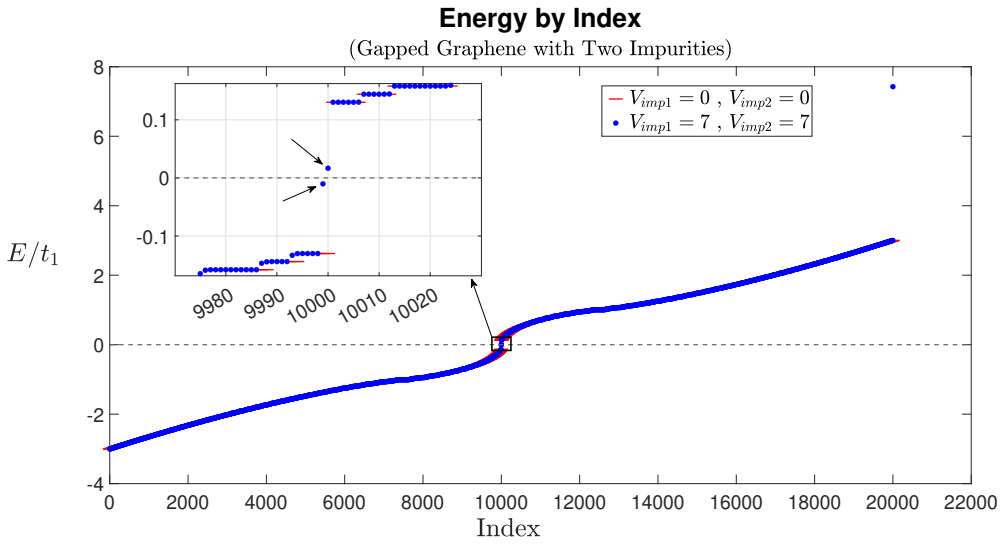

Figure 2.25: Energy by Index for two impurities.

Similar to graphene analysis, We observed variations in energy distribution once more while keeping a constant distance between two impurities. For the sake of comparison between the effects of single and two impurities on energy levels around $E = 0$, they are plotted on the same graph in Fig.2.26. In a manner similar to the graphene case, it is again observed that the single impurity state splits into a pair of impurity states due to the

presence of the second impurity.

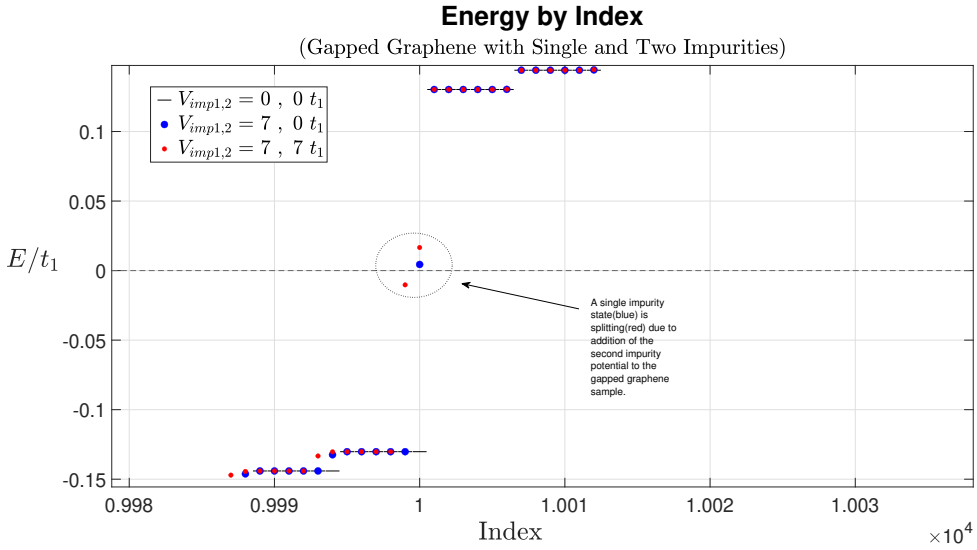

Figure 2.26: Energy by Index for gapped graphene for both single and two impurities.

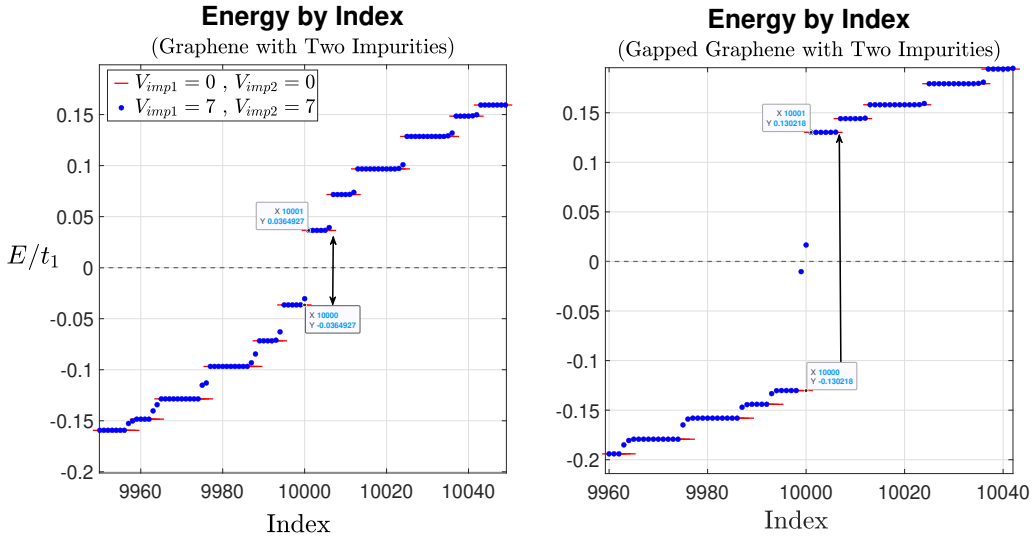

Figure 2.27: Energy by index comparison of graphene and gapped graphene.

Energy by index comparison of graphene and gapped graphene is shown in Fig. 2.27. The opened gap can easily be observed due to $\Delta\varepsilon$ which is the energy difference between sublattices A and B.

DOS has been affected mainly around Dirac point as observed in the graphene study. The formation around $E = 0$ can be observed for increasing distance between impurity potentials as seen in Fig. 2.28.

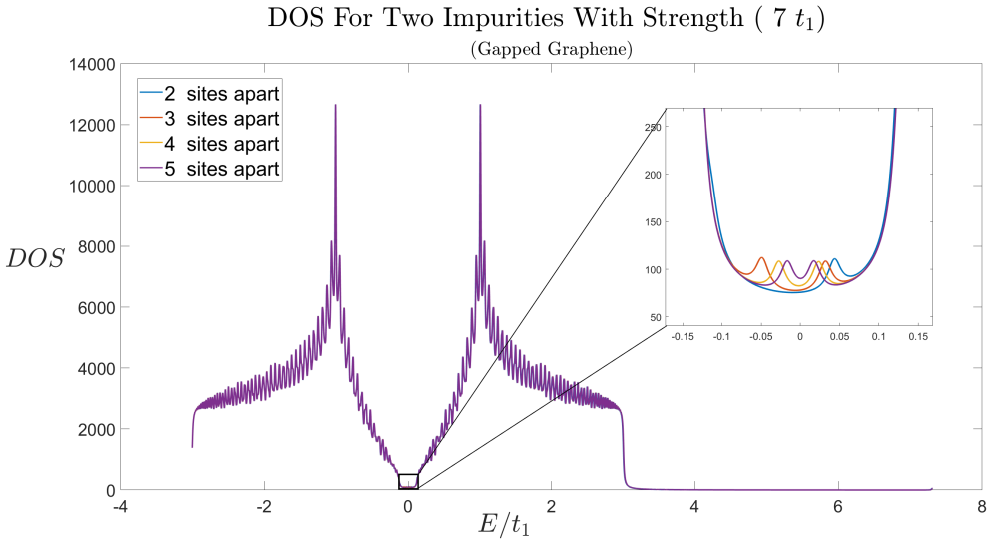

Figure 2.28: Spectrum of DOS of gapped graphene for 4 different distances between $V_{imp1} = 7t_1$ and $V_{imp2} = 7t_1$.

For gapped graphene, Fig. 2.29 shows the localized impurity states (No: 10000 and 9999) due to impurities ($V_{imp1} = V_{imp2} = 7t_1$) located randomly to the A-sites of the sheet along with the edge states (No: 20000 and 19999).

The energy and PR of a doublet are shown in Fig. 2.30 for the potential strengths from $1t_1$ to $10t_1$ and for the distances due to the movement in the armchair direction. In contrast to the graphene findings, increasing distance causes a rapid decrease of the energy difference of E^- and E^+ and a similar pattern for PR as well.

To see the implications of presence of two impurities the detailed plot for the energies of the states around Dirac point is again produced for gapped graphene. The energies of the splitting state emerged in bandgap meets to the same level rapidly compared to the other three doublets while the distance is increasing between the impurities, Fig.2.31.

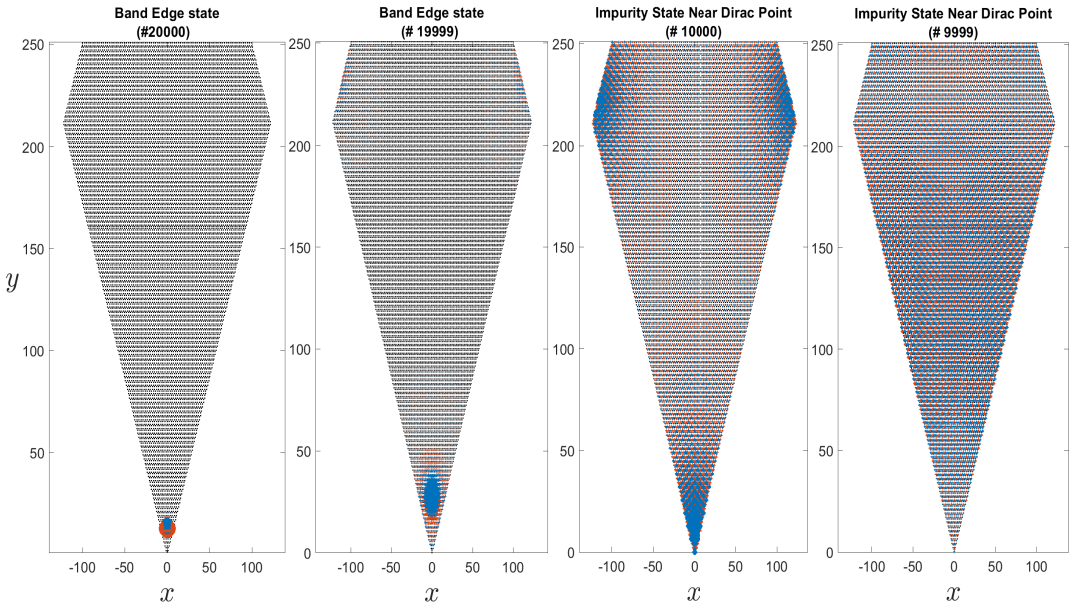

Figure 2.29: Representations in the real space lattice with state no. 20000, 19999, 10000, and 9999 for the strength $V_{imp} = 7t_1$. The + (blue) and - (red) values are reflected as the circle sizes.

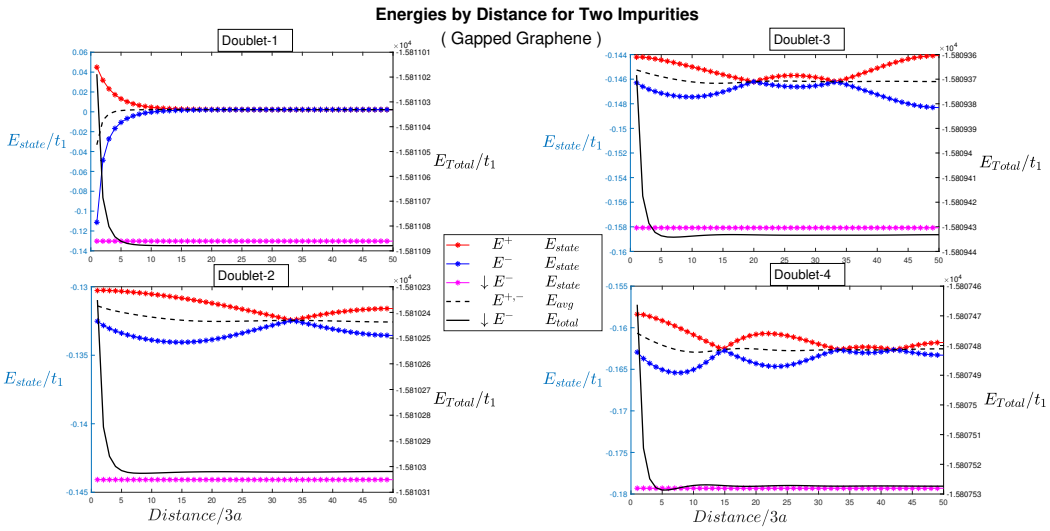

Figure 2.31: Energy by distance for four doublets around the Dirac point.

The total energy is calculated for the doublets around the Dirac point in the same manner by setting E_F related to the energies of the states as $E_F < E^-$; $E_F > E^+$; $E^- < E_F < E^+$. The total energy by distance graphs for Doublet-1 and Doublet-2 are shown in Fig.2.32.

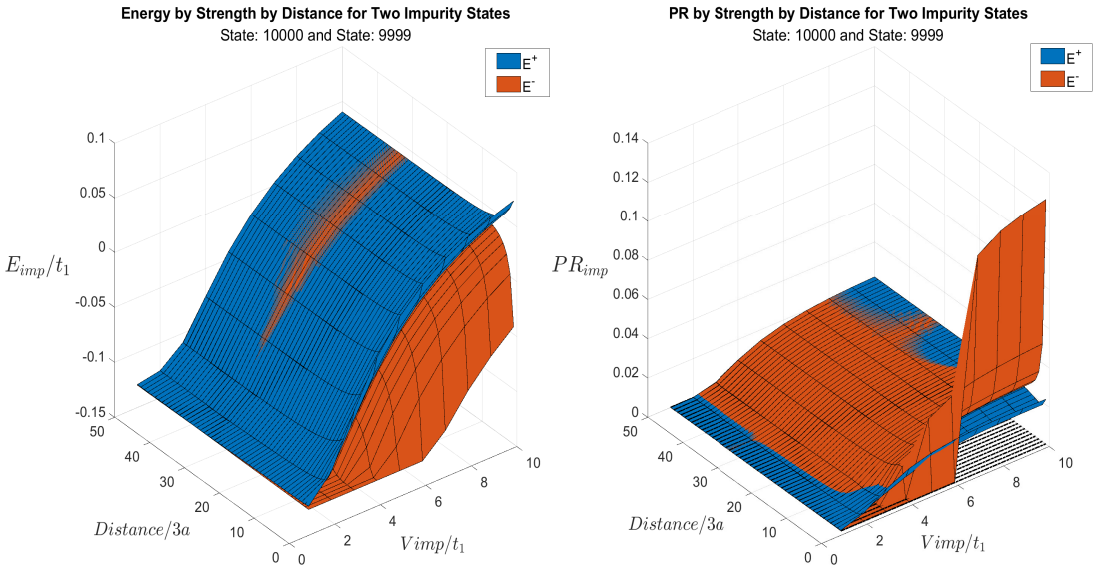

(a) Viewing

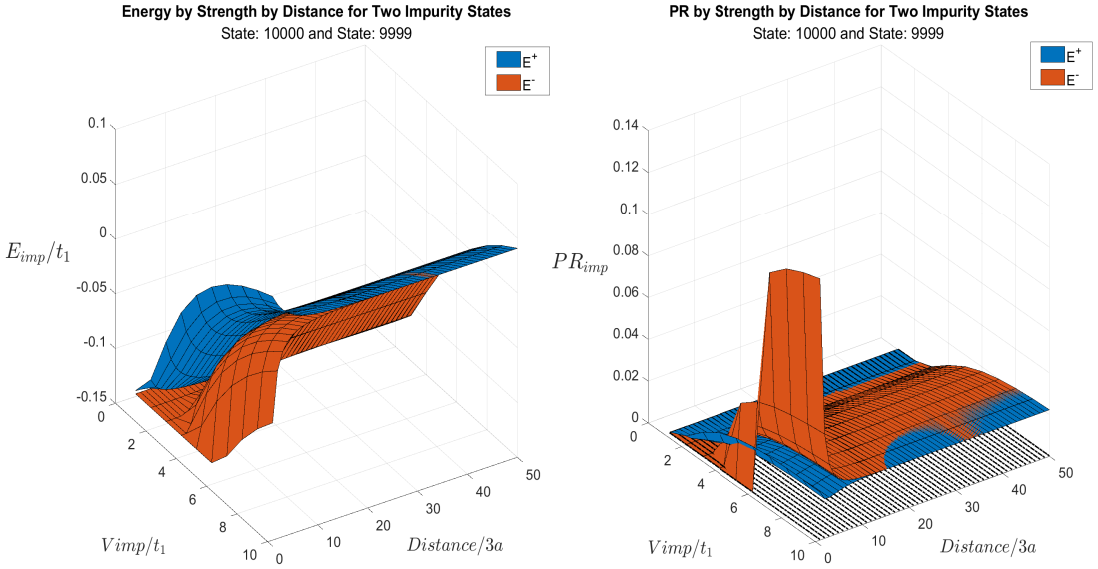

(b) Viewing Angle-2

Figure 2.30: Impurity State Energy and PR by impurity potential strengths between $0-10t_1$ and by distance between V_{imp1} and V_{imp2} for two viewing angles.

In the presence of two impurities for gapped graphene, the calculated forces for Doublet-1 and Doublet-2, around Dirac point, are plotted in Fig.2.33 where Doublet-1 has higher PR than Doublet-2. The force vanishes at large distances in all cases. For the situation $E^- < E_F < E^+$, only the bonding orbital is occupied, thus the force is attractive for sufficiently large impurity potentials for Doublet-1. When $E_F < E^-$, which implies that all impurity pairs are occupied, the force is of repulsive character for sufficiently strong impurity potentials. The force strength is rapidly decreasing with increasing distance as

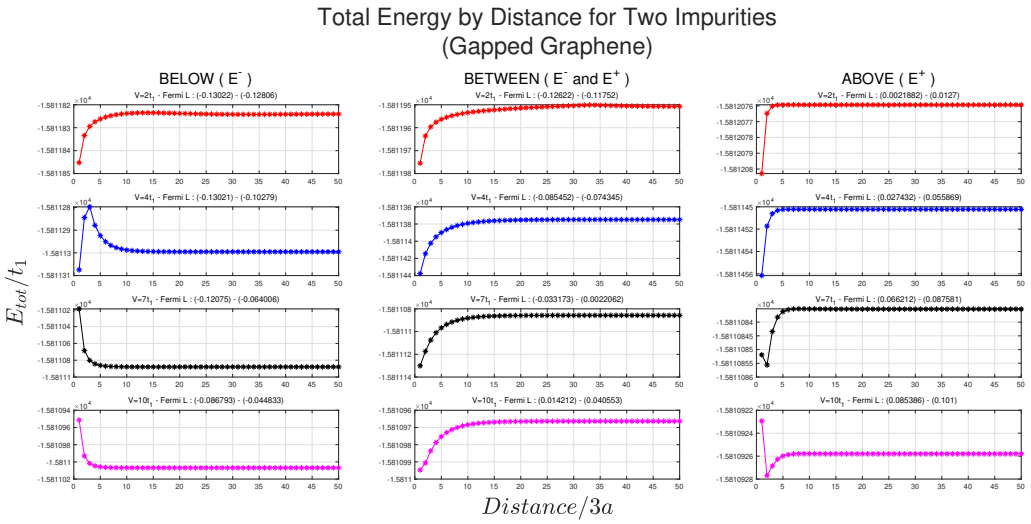

(a) Total Energy in the vicinity of Dirac point: Doublet-1

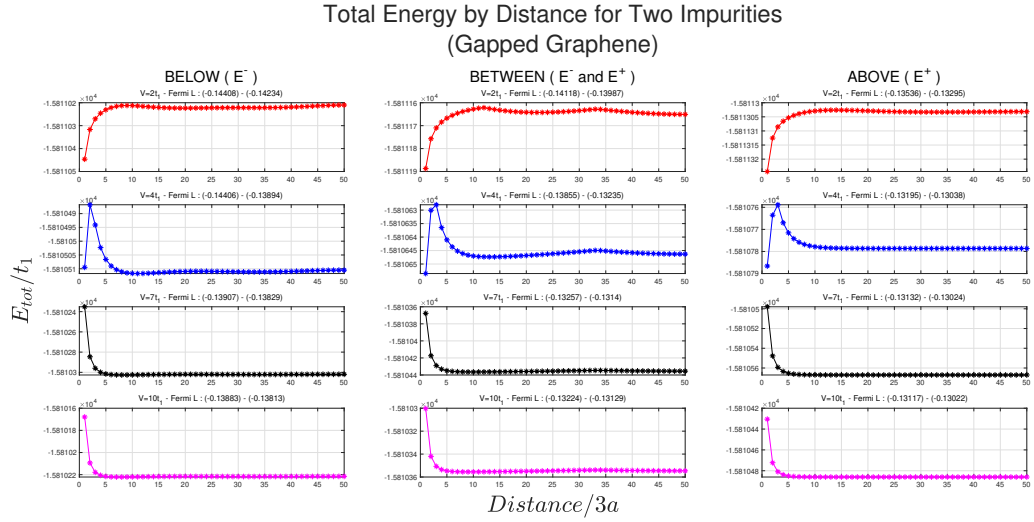

(b) Total Energy in the vicinity of Dirac point: Doublet-2

Figure 2.32: Total energy by distance for several potential strengths where E_F is set in the vicinity of two impurity states.

expected in the case of $E_F > E^+$. For Doublet-2 case, Fig. 2.33b, Fermi velocity is non-zero. This leads to Friedel oscillations in total energy and force as well. Note that Friedel oscillations are absent in Fig. 2.33a when Fermi wavevector is zero.

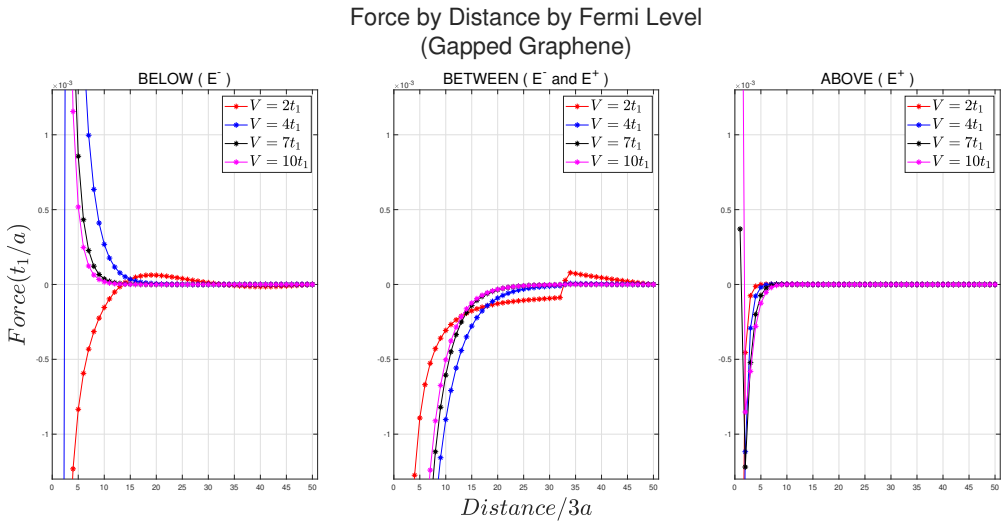

(a) Force by distance: Doublet-1

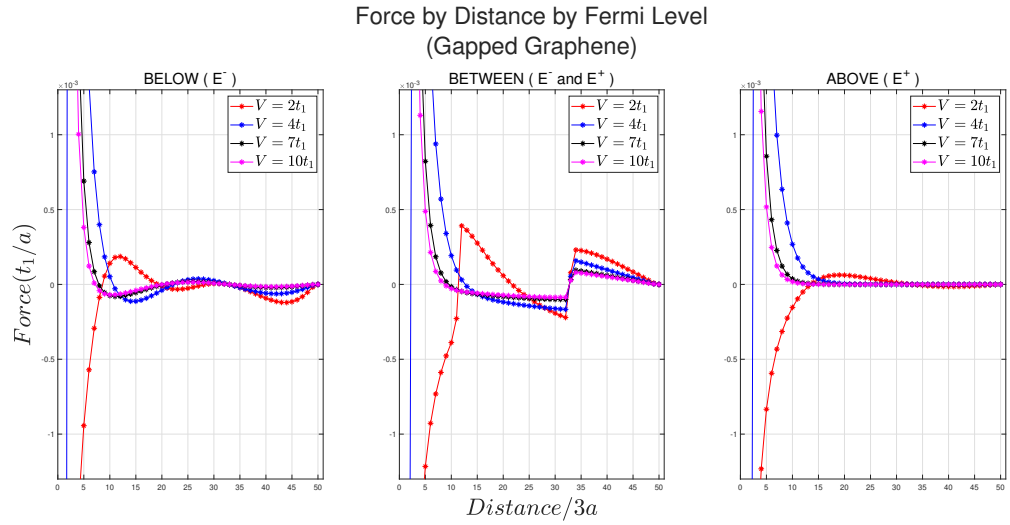

(b) Force by distance: Doublet-2

Figure 2.33: The force between impurity states for three different Fermi levels are calculated. In each figure, the impurity strengths, $2t_1$, $4t_1$, $7t_1$, and $10t_1$, are added together for comparison.

The forces for the doublets near Dirac point are drawn in Fig.2.34 emphasizing the impurity strengths where Fermi energy is set as $E_F < E^-$, $E^- < E_F < E^+$ and $E_F > E^+$.

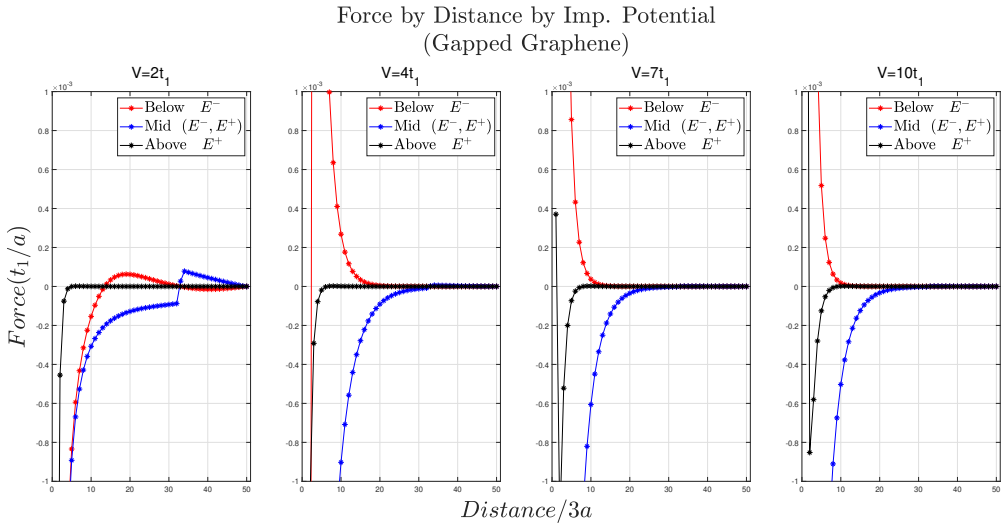

(a) Force by distance: Doublet-1

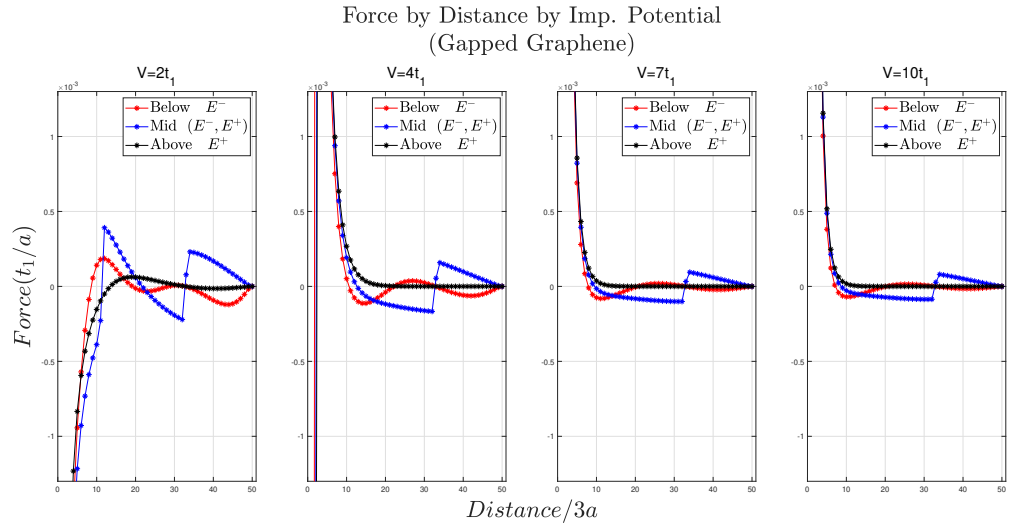

(b) Force by distance: Doublet-2

Figure 2.34: The force between impurity states for four different impurity strengths are calculated. In each figure, Fermi levels; $E_F < E^-$, $E^- < E_F < E^+$ and $E_F > E^+$ are combined in the plot for comparison.

CHAPTER 3

Conclusion

Throughout this thesis, we have conducted a systematic study of the influence of single and dual impurity potentials on the electronic properties of two-dimensional (2D) materials, with a special focus on graphene and gapped graphene. In the case of single impurity in graphene, a highly localized impurity state is identified at the band edge. Besides from this state, relatively less localized family of impurity states near Dirac point are identified. Similarly, for gapped graphene, again a highly localized state is observed at the band edge. Then, the following most localized state arises at the mid-bandgap, as well as a family of impurity states at the valance or conduction band depending on the sign of the impurity potential relative to hopping constant. We have investigated localization of the impurity states by studying the participation ratio, an indicative quantity for identifying localization. When two impurity potentials are introduced, it is observed that total energy of the system, both for graphene and gapped graphene, changes with the distance between two impurities. This implies a force between the impurities mediated by the Fermi sea. Further, we have investigated cluster of two impurity states. It is observed that the single impurity states split into a doublet of bonding/anti-bonding type orbitals with an energy difference changing with impurity-impurity distance. The highly localized states at the band edge are insensitive to the distance between the impurities and their value remains close to that of single impurity state. For the case of graphene, the family of doublets arise near the Dirac point. These doublets have an energy splitting highly dependent on impurity-impurity distance. In the case of gapped graphene, doublet at the mid-gap has the highest splitting. The family of doublets at the valance band also depend on the impurity-impurity distance, albeit weakly compared to mid-gap state. The energy of doublets converges to the single impurity energy value as impurity-impurity distance goes to infinity. We calculated the PR for impurity doublets as a function of impurity-impurity distance and impurity potential strength. We have seen a high correlation between the PR and force. We investigated the force when Fermi energy is $E_F < E^-$, $E^- < E_F < E^+$ and $E_F > E^+$. For strong enough impurity potentials, force is of attractive character when only bonding orbital of the doublet is occupied. When Fermi energy is bigger than the energy of the anti-bonding orbital the force rapidly dies off with distance. However total energy and force as well exhibit Friedel oscillations when the Fermi wavevector is non-zero.

REFERENCES

H. P. Boehm, R. Setton, and E. Stumpp. 1994. Nomenclature and terminology of graphite intercalation compounds. *Pure and Applied Chemistry* 66, 9 (1994), 1893–1901.

A. H. Castro Neto, F. Guinea, N. M. R. Peres, K. S. Novoselov, and A. K. Geim. 2009. The electronic properties of graphene. *Rev. Mod. Phys.* 81 (Jan 2009), 109–162. Issue 1. https://doi.org/10.1103/RevModPhys.81.109

Andre Geim and Konstantin Novoselov. 2007. The rise of graphene. *Nature Materials* 6 (2007), 183–191.

J. A. Lawlor, S. R. Power, and M. S. Ferreira. 2013. Friedel oscillations in graphene: Sublattice asymmetry in doping. *Physical Review B - Condensed Matter and Materials Physics* 88, 20 (nov 2013). https://doi.org/10.1103/PhysRevB.88.205416

S. Lebohec, J. Talbot, and E. G. Mishchenko. 2014. Attraction-repulsion transition in the interaction of adatoms and vacancies in graphene. *Physical Review B - Condensed Matter and Materials Physics* 89, 4 (jan 2014). https://doi.org/10.1103/PhysRevB.89.045433 arXiv:1311.1796

K. S. Novoselov, A. K. Geim, S. V. Morozov, D. Jiang, Y. Zhang, S. V. Dubonos, I. V. Grigorieva, and A. A. Firsov. 2004. Science. 306 (2004), 666.

Yotsarayuth Seekaew, Onsuda Arayawut, Kriengkri Timsorn, and Chatchawal Wongchoosuk. 2019. Chapter Nine - Synthesis, Characterization, and Applications of Graphene and Derivatives. In *Carbon-Based Nanofillers and Their Rubber Nanocomposites*, Srinivasarao Yaragalla, Raghvendra Mishra, Sabu Thomas, Nandakumar Kalarikkal, and Hanna J. Maria (Eds.). Elsevier, 259–283. https://doi.org/10.1016/B978-0-12-813248-7.00009-2

Andrei V. Shytov, Dmitry A. Abanin, and Leonid S. Levitov. 2009. Long-range interaction between adatoms in graphene. *Physical Review Letters* 103, 1 (aug 2009). https://doi.org/10.1103/PhysRevLett.103.016806 arXiv:0812.4970

Bruno Uchoa and A. H. Castro Neto. 2007. Superconducting States of Pure and Doped Graphene. *Phys. Rev. Lett.* 98 (Apr 2007), 146801. Issue 14. https://doi.org/10.1103/PhysRevLett.98.146801

P. R. Wallace. 1947. The Band Theory of Graphite. *Phys. Rev.* 71 (May 1947), 622–634. Issue 9. https://doi.org/10.1103/PhysRev.71.622

T.O. Wehling, M.I. Katsnelson, and A.I. Lichtenstein. 2009. Adsorbates on graphene: Impurity states and electron scattering. *Chemical Physics Letters* 476, 4 (2009), 125–134. https://doi.org/10.1016/j.cplett.2009.06.005

T. O. Wehling, K. S. Novoselov, S. V. Morozov, E. E. Vdovin, M. I. Katsnelson, A. K. Geim, and A. I. Lichtenstein. 2008. Molecular doping of graphene. *Nano Letters* 8, 1 (Jan. 2008), 173–177. https://doi.org/10.1021/nl072364w